UiT
THE ARCTIC
UNIVERSITY
OF NORWAY

Department of physics and technology

Plasma cloud detection and diagnostics from arcing by conditional averaging

—

Kenneth Nilsen

FYS-3931 Master's Thesis in Space Physics
June 2017

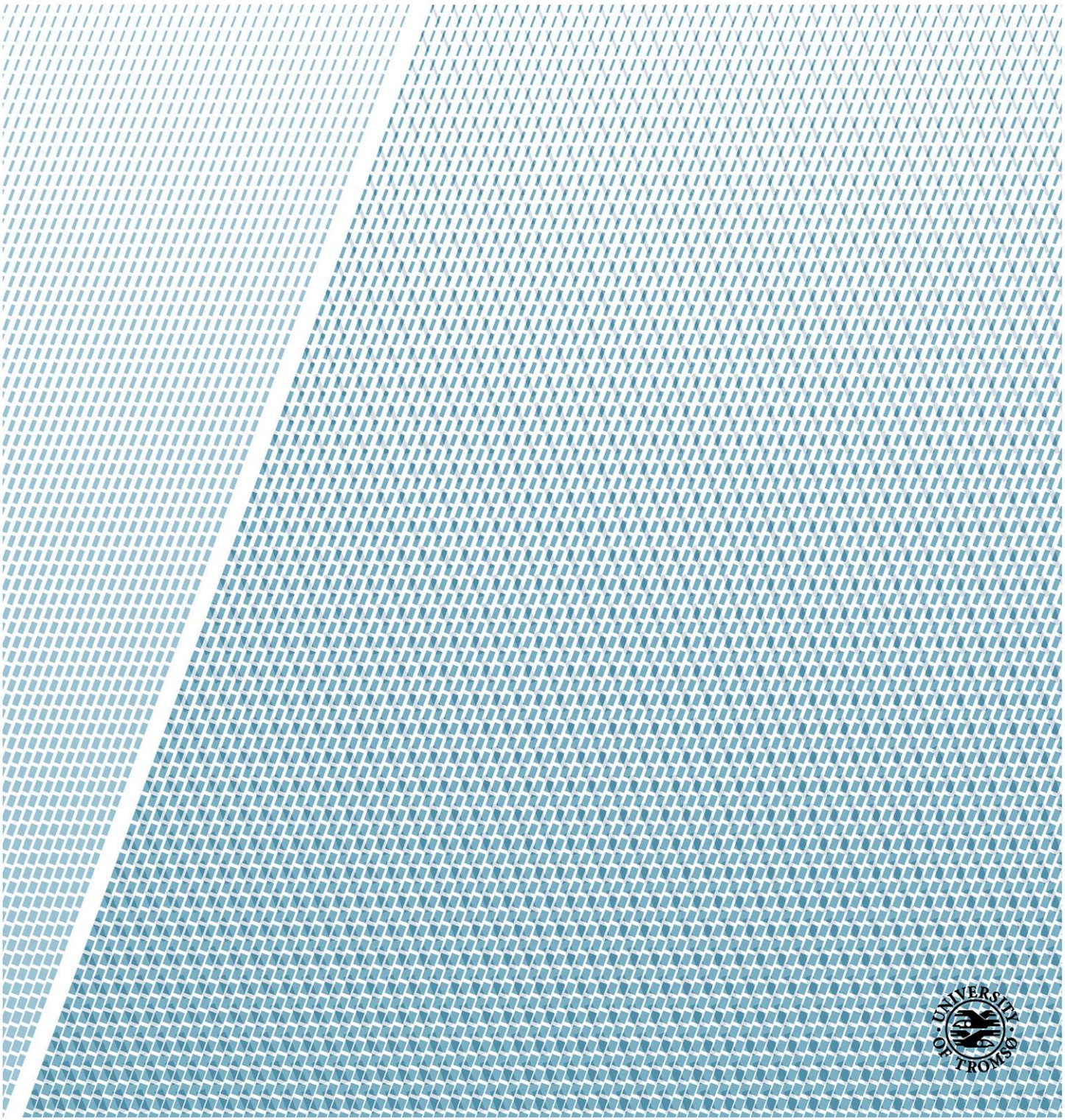

Abstract

Plasma cloud formation from arcing is experimentally studied. The arcs are formed by a high voltage set-up in the space simulation chamber at UiT. The plasma clouds are observed as large structures in the time series recorded by Langmuir probe and reference probe. By using the method of conditional averaging, the structures are accentuated.

The electron cloud formed by arcing was found to be characterized by a steep drop from zero current to a minimum, then relaxation towards zero current. Additionally, we found the magnitude of the amplitude to the electron cloud to be decreasing when the distance between the arc and the movable probe is increased. The average electron cloud velocity was found to be $\bar{v}_e = 1.32 \cdot 10^6\ ms^{-1}$.

The ion cloud formed by arcing was found to be characterized by a current above the steady state, which then increases logarithmically to a maximum, and then relaxes back to the steady state. However, the ion cloud measurement revealed a negative spike before the ion cloud, which indicates the electrons from an arc are energetic enough to be recorded by a negatively biased probe. The average ion cloud velocity was found to be $\bar{v}_i = 119.2\ ms^{-1}$, however the uncertainty was large due to high scattering.

During the experiment, we discovered that breakdown of gas causes an arc-like behaviour of the electrons. By applying the method of conditional average, a distortion was revealed. This result led us to a new condition that revealed that a high voltage breakdown gives rise to an electron cloud with the velocity $v_H = 7694ms^{-1}$, while the low voltage breakdown give rise an electron cloud with the velocity $v_L = 5441ms^{-1}$. Additionally, the amplitude of the electron cloud from the high voltage breakdown were significantly larger than he lower breakdown voltage. It is apparent the higher breakdown voltage creates a more energetic electron cloud than a lower breakdown voltage.

Acknowledgement

I wish to thank my supervisor, Åshild Fredriksen for all the help I was given throughout the work with my thesis.

I also wish to mention my friends who gave me support.

Contents

1 Introduction **1**

2 Background theory **3**
2.1 Electron emission . . . 3
2.1.1 Thermionic emission . . . 3
2.1.2 Photoelectric emission . . . 4
2.1.3 Field emission . . . 4
2.1.4 Thermal runaway . . . 6
2.1.5 Secondary emission . . . 6
2.1.6 Combination emissions . . . 7
2.2 Electrical discharges . . . 8
2.2.1 Dark discharges . . . 9
2.2.2 Glow discharges . . . 16
2.2.3 Arc discharges . . . 17

3 Method **19**
3.1 Sampling process . . . 19
3.2 Condition . . . 19
3.3 Conditional time Window . . . 20
3.3.1 Example: conditional time series . . . 21
3.3.2 Overlapping events . . . 21
3.4 Conditional analysis . . . 22
3.4.1 Example: conditional averaging . . . 22

4 Experimental set-up and recording **25**
4.1 Experimental set-up in SSC . . . 25
4.2 Arcing in SSC . . . 27
4.3 Arc recording . . . 28
4.3.1 Conditional recording . . . 28
4.3.2 Measurement grid . . . 29

5 Results and investigation **31**
5.1 Arc analysis . . . 32
5.1.1 Electron arc analysis . . . 32
5.1.2 Ion arc analysis . . . 37
5.2 Breakdown analysis . . . 41
5.2.1 Electron Breakdown . . . 41

6 Concluding remarks **47**

A Appendix **49**
A.1 Matlab Codes for Conditional Averaging 49
A.1.1 Conditional time interval 49
A.1.2 Conditional averaging 49

1 Introduction

For several decades, the spacecrafts Wind and STEREO, have recorded spike-like waveforms by the Time Domain Sampler from their antennas [16]. At first, the spikes were assumed to be some interference, but later, ideas were pursued that these spikes could be due to dust impact [16]. This idea arise from the work by [10] where they learned that hyper-velocity impact releases enough energy to induce plasma on the impact site that expands spherically, which is observed as a spike on spacecraft antennas. This interpretation was verified when an optical image on the spacecraft STEREO observed a debris simultaneous with spike signals on its antennas [16].

Many experiments based hyper-velociy impact between dust and plate [10, 5, 2, 3, 24, 25, 4, 15] and numerical simulations [8] were conducted to study the plasma cloud formation and its properties from hyper-velocity impact on materials.

It is of great interest to further study this phenomena, but hyper-velocity particle impact on surface is a difficult experiment to conduct without the proper tools. However, in [27] they conducted an experiment to see if arcing could simulate the voltage spikes as observed by the satellites. By using a satellite antenna with floating potential, they found the shape of the voltage spike from arcing to be somewhat similar to those observed by spacecraft during a high velocity impact. There is little research performed in this field, hence little is known regarding plasma emission due to arcing. This leads to the main objective of this thesis; to detect and diagnose the plasma cloud formed by arc discharges between a needle anode and a cathode, by means of conditional averaging. The analysis we will perform is to characterize the shape of the plasma cloud and estimate its velocity. This thesis is organized as follows:

Chapter 2 An introduction and discussion to electron emission and electrical discharges are given.

Chapter 3 An introduction and discuession to the method of conditional averaging are given.

Chapter 4 The experimental set-up and conditional sampling are described.

Chapter 5 Results from the experiment are presented and investigated

Chapter 6 Concluding remarks regarding the findings from the experiment

Appendix The matlab codes used to compute the conditional averaging are shown and discussed.

2 Background theory

In chapter **??**, I mentioned how [27] created plasma clouds by means of arcing with similar characteristics as plasma clouds created by dust impacts. Having a decent understanding of formation of arcs is thus of great importance in this thesis. This chapter will accordingly explain how arcs are formed.

In section **??**, we will look into the most important electron emissions for arcing and in section **??** we will look into the processes leading up to the arcing and how the electron emissions play their role.

2.1 Electron emission

Pure metals are materials that contains weakly bound valence electrons. The property of being weakly bound allows the valence electrons to move freely within the metal, but they cannot leave it. They are trapped within a potential well with a depth equal to the work function ϕ [26]. In this section, we discuss some of the physical processes and the combination of those that allows electrons to overcome this potential well. We will discuss the following processes

- Thermionic emission
- Photoelectric emission
- Field emission
- Thermal Runaway
- Secondary emission
- Combination emissions

2.1.1 Thermionic emission

By heating the metal to a high enough temperature ($T \geq 1000K$ [26]), the most energetic electrons of the Fermi-Dirac distribution may receive enough thermal energy to overcome the potential well ϕ of the metal, and escape [26, 1]. The electron current density emitted from the metal surface by this thermionic emission is described by the Richardson equation [26, 1]

$$J = AT^2 \exp\left(-\frac{e\phi_T}{K_B T}\right) \qquad \left[Am^{-2}\right] \tag{2.1}$$

where T is the temperature of the metal surface, e is the electron charge, ϕ_T[1] is the work function, K_B is the Boltzmann constant. The constant A is the Richardson constant given by [26, 1]

$$A \approx \frac{4\pi m_e e K_B^2}{h^3} = 1.2 \cdot 10^6 \qquad \left[Am^{-2}K^{-2}\right] \tag{2.2}$$

where h is Planck's constant, m_e is the electron mass. However, A is inconsistent with experiments due to different values for some metals [26]. For more details regarding equation (**??**), and the constants A and ϕ_T see [26].

2.1.2 Photoelectric emission

Photons may cause electron emission from solids by the photoelectric effect [26, 11]. This process only occurs if the photons has a frequency, ν above the photoelectric threshold, ν_{min} given by [26]

$$\nu_{min} = \frac{e\phi}{h} \qquad [Hz] \tag{2.3}$$

The energy of electrons emitted from a surface is given by Einstein's photoelectric equation [26]

$$E_e = h(\nu - \nu_{min}) \qquad [J] \tag{2.4}$$

where $\nu > \nu_{min}$. This process is shown in figure **??** where a single photon with energy E_p knocks out an electron from the surface with the energy E_e. By assuming that the incident photon has a frequency $\nu = \nu_{min}$, and a power flux $S\left[W/m^2\right]$ then the electron current density, J is given by [26]

$$J = e\Gamma_e = e\left(\frac{S}{e\phi}\right) = \frac{S}{\phi} \qquad \left[Am^{-2}\right] \tag{2.5}$$

2.1.3 Field emission

If a solid metal or a dielectric medium is exposed to a sufficiently strong electric field[2], then electrons may be pulled out of the solid's surface by electrostatic forces [26, 7, 6]. Consider two electrodes (e.g. parallel plates) with the potential difference V and the distance d between them. The critical electric field, E_C is the electric field necessary to cause field emission, given by [7]

$$E_C = \frac{\beta V}{d} \qquad \left[Vm^{-1}\right] \tag{2.6}$$

[1] ϕ_T is the work function of the metal that must be added to an electron at $T = 0$ [26]

[2] For metals, the necessary electric field strength is found to be in the order of $\sim 10^9 V/m$ to create field emission [7]

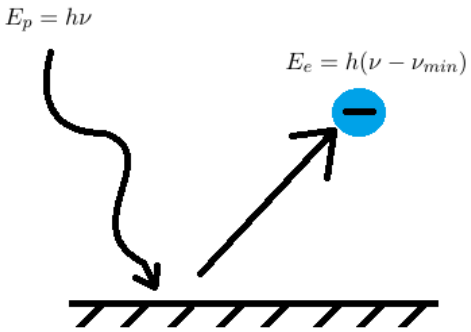

Figure 2.1: Illustration of a single electron emission by photoelectric effect by one photon from a surface

Where β is the local field factor. The magnitude of electrostatic forces required to cause field emission is very high, which demands a very high voltage. This can be achieved by either using a very powerful high voltage power supply or one can reduce the distance d between the electrodes. However, even with a very small distance say $d = 1mm$, the required voltage is still $V = 10^6$. These parameters are not easy to operate with, hence one can instead increase the local field factor, β. The β factor accounts for all advantages given to equation (**??** such as geometry, material and etc [7, 1]. However, The β factor is mostly used for geometric enhancements e.g. sharp edges, protrusions, step defects and so on [7, 1]. Figure **??** shows an example of the equipotential lines and electric field strength around a sharp point.

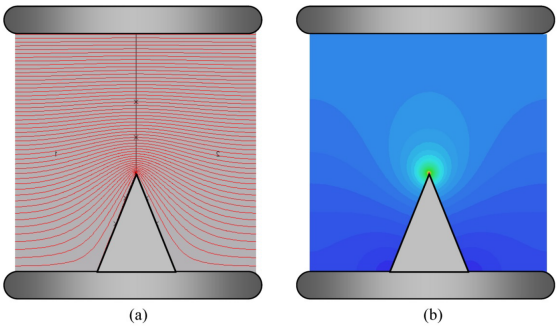

Figure 2.2: Equipotential lines (a) and electric field strength (b) around a sharp point (fig. 12 from [6])

From experiments in vacuum, the β factor is found to be in the range of 10-100, but in some extreme cases it has been found to be in the order of 10^3 [7, 1]. This factor is a large contribution to equation (**??**).

Sometimes electrons may be emitted by field emission even though the electric field is not sufficiently high. This is explained by quantum tunnelling [26, 7, 6]. By treating the

electron inside the metal as a wave inside a potential well, there is a finite probability for the wave to overcome the potential well. This quantum tunnelling process was studied by Fowler and Nordheim in 1928 [26, 7], and later in 1933, Fowler managed to derive the field emission current density

$$J_f = CE^2 \exp\left(-\frac{D}{E}\right) \qquad \left[Am^{-2}\right] \tag{2.7}$$

where E is the electric field strength, C and D are constants that have to be determined and depend on the material used. Details regarding this equation and the constants can be found in [26].

2.1.4 Thermal runaway

If a solid metal surface is subjected to a plasma, then most of the voltage drop occurs in a very thin plasma sheath between the plasma and the metal surface [26, 18, 1]. This sheath is usually a few electron Debye lengths[3] wide. Given a thin plasma sheath (order of 10^{-4}m [18]), then a small potential can give rise to a very strong electric field [18, 26]. This type of emission is also supported by the β factor such as sharp edges or protrusions as explained in the previous section [1].

2.1.5 Secondary emission

When ions with sufficient energy impacts the cathode, the cathode may emit an electron [26, 18]. This process is also referred to as sputtering, and characterized by the secondary electron emission coefficient given [26, 18]

$$\gamma_e = \frac{\text{number of electrons emitted}}{\text{number of ions incident on cathode surface}} \tag{2.8}$$

If the ions impacting the cathode have energy levels in keV range, then γ_e may be greater than one, hence more than one electron may be emitted per incident particle [26]. Secondary electrons may also be emitted from the anode by energetic electron impact [26]. Secondary emission process is shown in figure **??**.

[3] Debye length is the average distance which the electrons redistribute themselves in within the plasma to keep the plasma overall quasineutral [18]

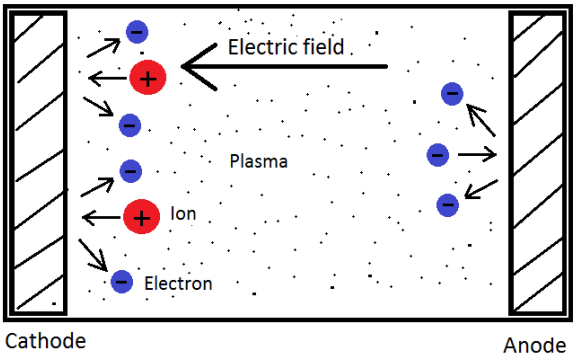

Figure 2.3: Illustration of secondary emission

2.1.6 Combination emissions

The different types of emission we have discussed so far can be combined into a more complex emission process. This section will give a brief introduction to some of these emissions relevant to our experiment.

Thermo-field emission

The combination of thermionic and field emission results in thermo-field emission [12, 1]. Contrary to the expectations, this emission is in fact greater than the linear superposition of the field and thermionic emission. It is approximated by [1]

$$J_{TF} \approx k\left(AT^2 + BE^{9/8}\right)\exp\left[-\left(\frac{T^2}{C}+\frac{E^2}{D}\right)^{-1/2}\right] \qquad \left[Am^{-2}\right] \tag{2.9}$$

Where E is the electric field and A, B,C and D are material specific constants [1]. More details regarding equation **??** is given in [12].

Schottky effect

The Schottky effect is thermionic emission assisted by an electric field (hence the other name field enhanced thermionic emission) [1]. The current density of this emission is the same as Richardson equation (**??**) except for the reduced work function due to the deformation provided by the electric field. To add the deformation contribution to the Richardson equation, we replace the work function ϕ with $\phi - \Delta\phi$, hence

$$J = AT^2 \exp\left(-\frac{e(\phi-\Delta\phi)}{K_B T}\right) \qquad \left[Am^{-2}\right] \tag{2.10}$$

Where $\Delta\phi$ is the deformation.

2.2 Electrical discharges

Electric discharge is a current flow through a dielectric medium in an applied electric field [26]. Some typical examples of electrical discharges are lightning in the skies, arcing between disconnected power lines, neon light signs, brush discharge from a single conductor, fluorescence light bulbs, Tesla coils and so on. In this section, the aim is to get a basic understanding on the processes that leads to an arc discharge.

Consider a simple set-up consisting of a evacuated (low pressure $\sim (0.1 - 10)$Torr [6, 26, 18]) glass tube of length L with a circular parallel plated electrode at each end [26, 18, 6]. The electrodes are connected to a high voltage DC power supply, making one electrode the anode and the other the cathode [26, 18, 6]. When the voltage is turned on, a uniform electric field will arise between the electrodes. The electric field accelerates the electrons towards the anode and the ions toward the cathode [26]. This movement of charges creates a current flow through the discharge, inside the tube [26]. This set-up with an electric field and moving ions and electrons are shown on figure **??**.

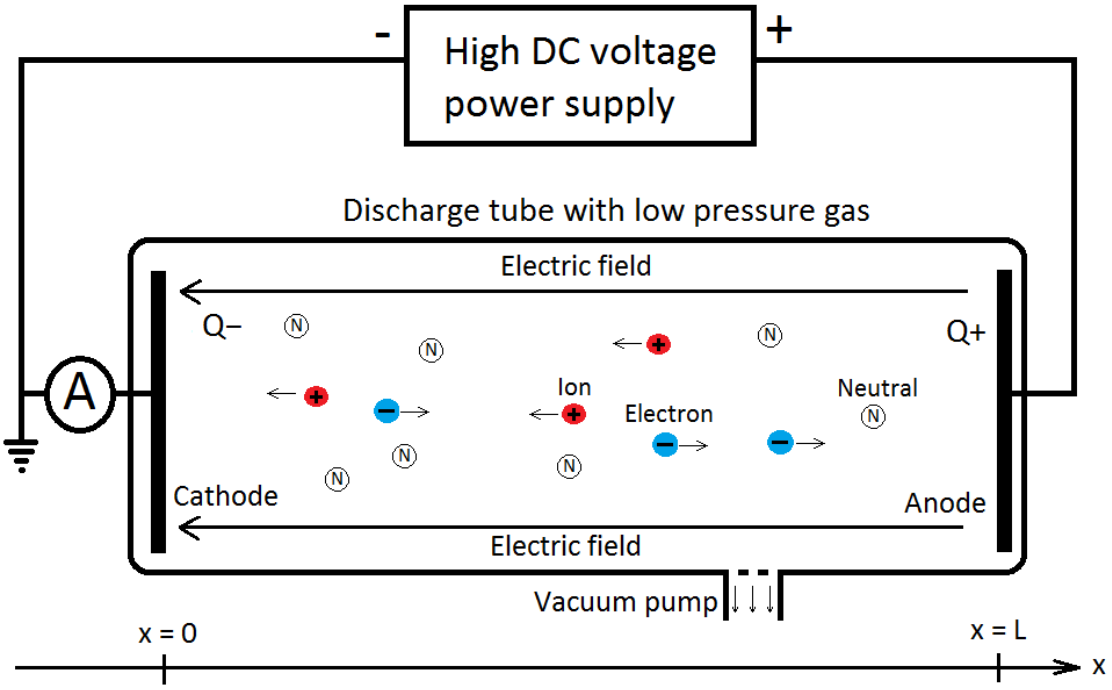

Figure 2.4: Illustration of the low pressure electrical discharge in a glass tube

By increasing the voltage while measuring the current flow through the discharge, one can plot voltage-current characteristics of the discharge [26, 18, 6]. General voltage-current characteristics is shown in figure **??**. However, the shape and curve of the voltage-current characteristics given by figure **??** depends on the pressure, gas species, magnetic field (if present) and electrode- material, temperature and geometry [6].

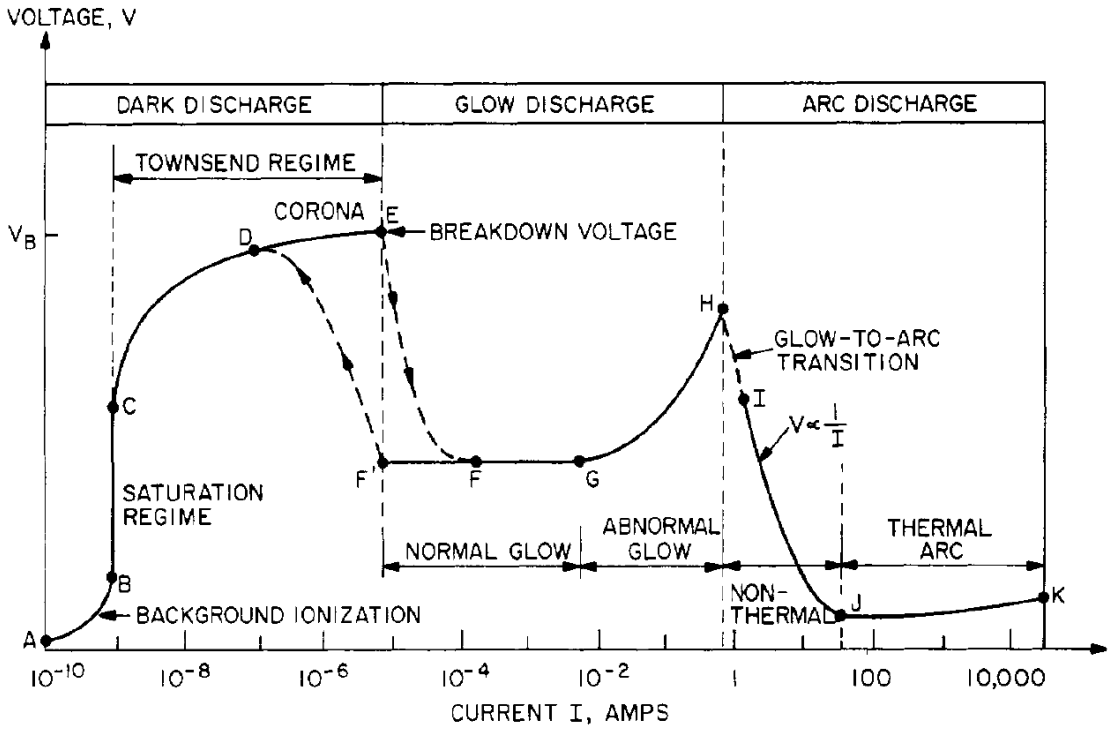

Figure 2.5: A general voltage-current characteristics for a DC electrical discharge (fig. 4.12 from [26])

2.2.1 Dark discharges

The dark discharges receives its name for being dark [26]. This is due to the low density of excited atoms in this discharge, such that there is not enough light emitted to be visible for human observers, sans the corona and the spark [26]. The regions in the dark discharge are summarised on the left side in figure **??**.

Background ionization

The first region we enter is the background ionization, which is between point A and B in figure **??**. In this region, the applied voltage creates an electric field between the electrodes that are suffcient to sweep out the free electrons and ions from the discharge volume. This process gives rise to a very small measurable current (in the order of 10^{-9}) [26, 6]. These free charges inside the discharge volume are created naturally by background ionization and radiation processes [26, 6],

Saturation

The second region is between B and C in figure **??** is the saturation region. In this region, an increase in voltage will result the same current as obtained at point B. This

is due to all charges from the discharge are saturated, hence there are no more charges available in the discharge to create more current [26, 6]. The saturation current, I_s in this region of figure **??** is given by [26].

$$I_s = ALe\frac{dn}{dt} \qquad [A] \tag{2.11}$$

where A is the cross-sectional area of the discharge, L is the length of the discharge, e is the elementary charge and dn/dt is the time derivative of the electron or ion density.

Townsend regime

The third region is the Townsend regime, located between C and E in figure **??**. An increase in voltage in this region will result in an exponential increase in current. This sudden current growth is explained as follows.

In the set-up given by figure **??**. we have electrons being emitted from the cathode due to secondary emission [26], which are accelerated toward the anode by the applied electric field. When the applied voltage is set to point C in figure **??**, the emitted electrons may gain sufficient energy to ionize a neutral particle, creating a new ion and a secondary electron, before they reach the anode [26, 6].

If we increase the applied voltage beyond point C in figure **??**, the emitted electrons and the secondary electron may obtain sufficient energy to ionize another neutral particle, creating another two more ions and two more secondary electrons, before they reach the anode [26, 6]. If we keep increasing the applied voltage, the number of electrons and ions will double from the previous voltage, resulting in an exponential increase in charges. This process is known as Townsend avalanche[4] and is illustrated in figure **??**.

For future discussions regarding electrical breakdown, it is necessary to derive the equation describing the current in the Townsend regime. The number of electrons in the Townsend regime were first derived by John Townsend in 1897 [26, 6]. Consider the geometry given by figure **??** where the cathode is located at $x = 0$ and emits a flux of electrons, Γ_{ec} [26]. The differential increase of electron flux, $d\Gamma_e$ from the ionization impact caused by the emitted electrons somewhere in the discharge $x, x + dx$ is given by [26]

$$d\Gamma_e = \alpha\Gamma_e dx \tag{2.12}$$

where $\alpha = \left[m^{-1}\right]$ is Townsend's first ionization coefficient, which is the average number of ionizing impact made by an electron as it travels one meter [26]. Furthermore, if there are no loss of electrons (e.g. no recombination) while they move along the discharge [26], then integrating from $x = 0$ to $x = L$ gives the total electron flux reaching the anode

$$\Gamma_{ea} = \Gamma_{ec}e^{\alpha L} \qquad \left[m^{-2}s^{-1}\right] \tag{2.13}$$

where Γ_{ec} is the electron flux emitted from the cathode. Equation (**??**) gives the total electron flux reaching the anode as function of distance, L between the electrodes.

[4] Townsend avalanche is also called electron avalanche in other literatures

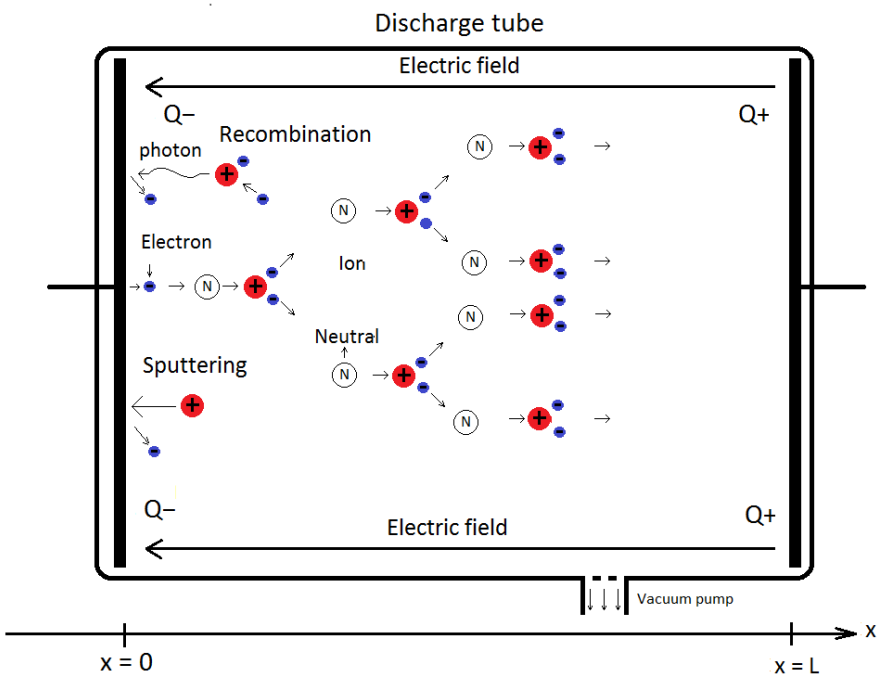

Figure 2.6: An illustration of the Townsend Avalanche

Given the set-up in figure **??**, then the relationship between distance and voltage is $V = EL$ where E is the applied electric field between the electrodes in figure **??**. Solving for the distance L and insert this into equation (**??**), we get

$$\Gamma_{ea} = \Gamma_{ec} e^{\alpha \frac{V}{E}} \qquad \left[m^{-2} s^{-1}\right] \tag{2.14}$$

which is the total electron flux reaching anode as function of applied voltage. We can find the total current, I_{ea} reaching the anode by multiplying both sides of equation (**??**) with the electron charge e and the cross-sectional area of the discharge A

$$I_{ea} = I_{ec} e^{\alpha \frac{V}{E}} \qquad [A] \tag{2.15}$$

Equation (**??**) describes the current as function of voltage in the Townsend regime. However, equation (**??**) is overly simplified since it considers the secondary emission as the only contribution to the electron flux from the cathode, Γ_{ec} [26]. A more accurate expression can be obtained by taking more contributions into account. We redefine the electron flux from the cathode, Γ_{ec} to be a sum of additional contributions [26]

$$\Gamma_{ec} = \Gamma_{es} + \Gamma_{eo} \tag{2.16}$$

where Γ_{es} is the electron emission from the cathode by secondary emission and Γ_{eo} is electron flux from the cathode due to all other effects such as photoelectric effect [26, 18]. Furthermore, to keep the system in steady state, the charge continuity must remain constant. That means, one electron emitted from the cathode creates one secondary electron and one ion through impact ionization, or in other words, the electron flux reaching the anode must be equal to the electron flux emitted by the cathode and the ion flux reaching the cathode [26, 18]. This gives

$$\Gamma_{ea} = \Gamma_{ic} + \Gamma_{ec} \tag{2.17}$$

where Γ_{ic} is the ion flux reaching the cathode, given by [26, 18]

$$\Gamma_{ic} = \frac{\Gamma_{es}}{\gamma} \tag{2.18}$$

where γ is the secondary electron emission coefficient, which is the number of electrons emitted from the cathode per incident ion or photon. This coefficient is defined by [26, 18, 6]

$$\gamma \equiv \frac{\text{number of electrons emitted}}{\text{number of incident ions or photons}} \tag{2.19}$$

The total electron flux reaching the anode, Γ_{ea} can be found by combining the equations (**??**), (**??**), (**??**) and (**??**) and solve for Γ_{ea}. This gives

$$\Gamma_{ea} = \Gamma_{eo} \frac{e^{\left(\alpha \frac{V}{E}\right)}}{1 - \gamma \left(e^{\left(\alpha \frac{V}{E}\right)} - 1\right)} \tag{2.20}$$

The total current reaching the anode is found by multiplying both sides of equation (**??**) with the electronic charge e and cross-sectional area of the discharge A

$$I_{ea} = I_{eo} \frac{e^{\left(\alpha \frac{V}{E}\right)}}{1 - \gamma \left(e^{\left(\alpha \frac{V}{E}\right)} - 1\right)} \qquad [A] \tag{2.21}$$

Equation (**??**) indicates that the current in the Townsend regime increases more rapidly than the prediction given by equation (**??**) [26]. Equation (**??**) will be further discussed in section **??**.

Streamer

Consider a Townsend avalanche somewhere in the middle of the discharge. Figure **??** shows the (a) distribution of the charged particles in the avalanche, (b) the charge density of the avalanche and (c) the electric field within the avalanche. In figure **??** (a) and (b) we observe the head of the avalanche, facing the anode, primarily consists of negative charges, while the tail consists of positive charge. This formation of the charges inside an avalanche arise from the fact the ions are much heavier than the electrons ($n_i/n_e \leq 1800$ [6]) thus the electrons are more efficiently accelerated by the applied

electric field between the electrodes than the ions. The electrons in the avalanche are accelerated by the applied field and creates additional free electrons through impact ionization with the neutral atoms while they travel towards the anode. Meanwhile, photons emitted by ions (due to recombination) and excited atoms (by relaxing into stable states), further ionize (or excite) neutral atoms, thus creating additional free electrons [6].

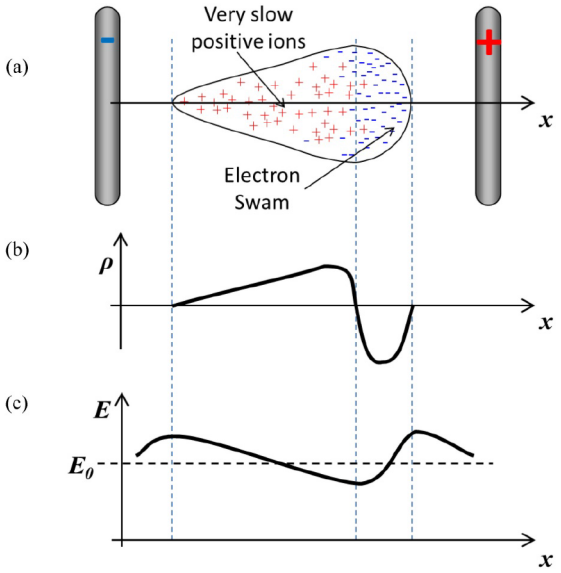

Figure 2.7: Illustration of the (a) distribution of particles, (b) charge density and (c) electric field in the distribution of a single avalanche (fig. 8 from [6])

Any free electrons created in the higher field regions in figure **??** (c) will go on to produce more additional avalanches from the initial avalanches head and tail (which are the higher field regions) [6]. If we manage to obtain additional avalanches from an initial avalanche, then we have a chain of avalanches, also referred to as streamers [6]. The formation of streamers are illustrated in figure **??**.

As the reader may be aware of, streamers consists of free charges with a high charge density, thus the streamers are a thin and highly conductive channel of plasma along an applied electric field, characterized by an intense light [6, 17], thus creating streamers means to cause an electrical breakdown[5] of gas.

Moreover, since we are using a needle as an anode in our experiment, it is necessary to discuss geometric enhancements for the streamers. Consider figure **??** where we have a sharp edge which causes the equipotential lines to bunch up on the tip, resulting in a geometric field enhancement. The polarity of the sharp edges with the creation of Townsend avalanches is summarized in figure **??**. In figure **??** (a) we observe the Townsend avalanches to be developing into an increasing electric field, making it easier

[5]Electrical breakdown is when a a dielectric medium is subjugated to a sufficiently high electric field the medium can break down and become electrical conductive [26, 11, 7, 6].

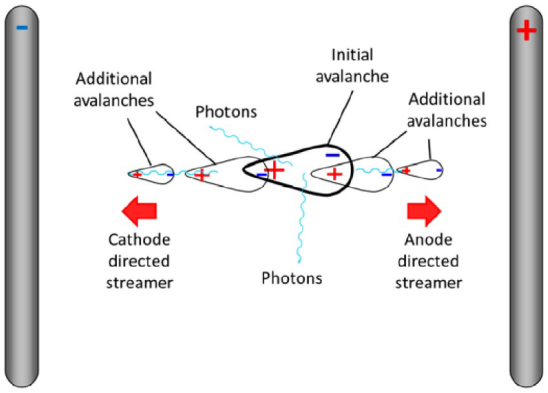

Figure 2.8: Formation of streamer by chain of avalanches (fig. 9 from [6])

for this avalanche to form streamers and propagate. In figure **??** (b) we observe the Townsend avalanches are developing in an decreasing field, making it much harder to form streamers and propagate.

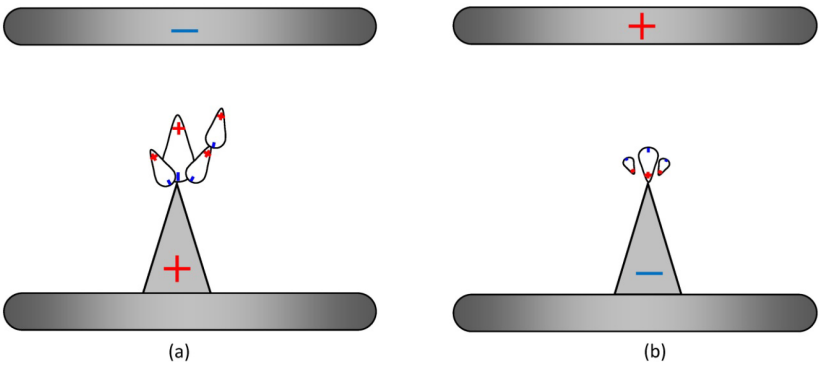

Figure 2.9: Townsend avalanches for (a) positive and (b) negative point-plane discharges for the same applied field (fig. 13 in [6]).

Corona

While we are in the Townsend regime, we may encounter the corona, located at point D in figure **??**. Corona is a partial discharge that arise when the streamer formation does not bridge the gap between the electrodes [26, 6]. However it causes an electrical breakdown of the surrounding gas, resulting in a luminuous brush-like discharge. The corona discharge usually arise from high local fields, e.g. from sharp edges, fine wires and so on [26]. Furthermore, this discharge could be characterized as a glow discharge, in sense that it needs an electron flux from the cathode by means of secondary emission, photo electric effect and so on, in order to be sustained [26, 18]. However, it differs from

the glow discharge by requiring a very high voltage and very low current, as observed in figure **??**.

Electrical breakdown

Electrical breakdown is the final point in the Townsend regime and the dark discharges, which is at point E in **??**. The voltage given at point E is the breakdown voltage[6] denoted V_B. This is the voltage required to make the streamers bridge the gap between the electrodes in the set-up given by figure **??** [6, 17]. When this occurs, we have a channel of highly conductive plasma between the electrodes, characterized as a spark, somethimes audible as a crack [6]. Furthermore, as soon as this channel is formed between the electrodes, a high current[7] is sent through the loop in figure **??**.

For the experiment we are conducting in this thesis, the breakdown voltage, V_B is essential. We continue with equation (**??**). When we have an electrical breakdown, the current given by equation (**??**) will increase rapidly [26, 6]. This means the denonimator in equation (**??**) goes to zero [26].

$$1 - \gamma(\exp^{\left(\alpha \frac{V_B}{E_B}\right)} - 1) = 0 \tag{2.22}$$

Equation (**??**) is known as the Townsend criterion [26, 6]. Taking the natural logarithm of equation (**??**) and divide on γ yields

$$\alpha \frac{E_B}{V_B} = \ln(\gamma + 1) \tag{2.23}$$

where α is Townsend's first ionization coefficient. The analytical solution to α can be found by computing the product of the mean free path, and the probability of an electron having a free path greater than an ionization distance [26, 18]

$$\alpha = pA \exp\left(-\frac{C}{E/p}\right) \tag{2.24}$$

where p is pressure, E is the electric field, A and C are constants determined experimentally [26, 18]. Details regarding the derivation of equation (**??**) and the constants A and C are given in [26, 18]. Furthermore, inserting equation (**??**) in (**??**) and solving for the breakdown voltage V_B yields

$$V_B = \frac{Cpd}{\ln(Apd) - \ln[\ln(1 + 1/\gamma)]} = f(pd) \tag{2.25}$$

One should note the breakdown voltage, V_B is stochastic due to the definition of α [6]. This means that if you obtain a breakdown at a certain voltage, you may not achieve another voltage at the same voltage, and additionally, no breakdowns are ever the same [6].

[6] Breakdown voltage is also referred to as sparking voltage
[7] in the order of $10^4 A$ to $10^8 A$ [26]

By plotting the equation (**??**) as a function of pd, then we obtain the Paschen curve [26, 18, 6]. Figure **??** shows the breakdown voltage for hydrogen as an example. By observing figure **??**, we notice the importance of the mean free path between collisions in order to create Townsend avalanches, e.g. If we have a high pressure, which corresponds to a short mean free path, then the electrons will not have the time to be properly accelerated by the applied electric field before they hit a neutral atom and loose its energy. The distance between the electrodes needs to be short to compensate the high pressure in order to achieve a breakdown [6]. In the other hand, if the pressure is low, which corresponds to a long mean free path, then the electrons will not hit anything before they reach the anode. To compensate for this, the distance between the electrodes needs to be sufficiently long such that the electrons manage to hit the neutrals and cause breakdown [6].

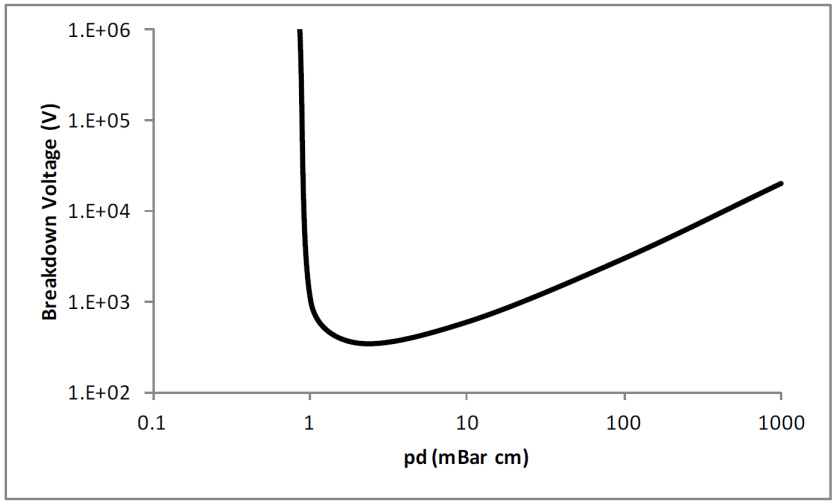

Figure 2.10: The Paschen curve for hydrogen (fig. 10 from [6])

However, one should note the Paschen curve varies heavily on the gas specie, e.g. the Paschen curve for Argon has its minimum at $pd = 0.1 mbar\ cm$ [6].

2.2.2 Glow discharges

The glow discharges are characterized by a low current, high voltage and for being luminous in contrast to the dark discharges (sans the corona and the spark) [26, 18]. However, just like the corona discharge, to keep the glow discharge sustained, it needs a continuous electron flux from the cathode by means of secondary emission, photoelectric effect and so on.

Given the set-up shown by **??** where we assume the internal resistance of the power supply is sufficiently low, then after an electrical breakdown at E in figure **??**, the discharge inside the set-up will make a discontinuous transition from the dark discharges to the glow discharges at point F in **??**.

Normal glow

The first region we enter in the glow discharges is the normal glow discharge, which is between the points F and G in figure **??**. This region is characterized by the voltage being independent of the total current flowing through the discharge tube and the current density reaching is independent of the total current [26]. This fact arise from the plasma in this region is in contact with only a small part of the cathode surface at low currents [26]. However, if we externally increase the current delivered to the cathode, then the contact area between the plasma and the cathode increases such that the total current is delivered at a constant current density [26].

If we increase the current delivered until the contact area between the plasma and cathode surface is equal to the cathode surface itself, we enter the abnormal glow at point G in figure **??**.

Abnormal glow

The second region after the normal glow is the abnormal glow, which is between G and H in figure **??**. At this point, the plasma covers the whole cathode surface, hence an increase in current will now result in an significant increase in voltage [26]. Additionally, an increase in current at this point will also increase the cathode temperature, which leads us to the arc discharges.

2.2.3 Arc discharges

Arc discharges are characterized by high current and low voltage, which corresponds to an intense luminosity and high temperature [26, 1]. The regions of the arc discharges are summarized on the right side in figure **??**, starting from the glow-to-arc transition at H.

Glow-to-Arc transition

We return to the abnormal glow at between the point G in figure **??**. If we deliver current to the cathode by external means, we will increase its heat load [26]. If we keep increasing the current delivered to some high value around point H in figure **??**, then the heat load on the cathode may become sufficient to cause thermionic emission as an additional electron emission from the cathode [26]. When this emission occurs the glow discharge will make the transition to the non-thermal arc in the arc regime and settle down at some point I, determined by the internal impedance of the power supply [26].

Non-thermal arc

After the glow-to-arc transition from point I in figure **??** we enter the non-thermal arc[8] region, which is characterized by its negative resistance relation, $V = R^{-1}I$ [26]. However, the non-thermal arcs cannot be sustained by the secondary emission, in fact,

[8]Non thermal arcs are also referred to as low intensity arcs, thermionic arcs or low pressure arcs

the current provided by secondary emission in this region is insignificant [26]. To sustain a non-thermal arc, we need additional electrons provided by the thermionic emission continuously.

Thermal arc

In figure **??** we observe the thermal arc region to be between the points J and K. This discharge is characterized by having a very high current and current densities, and a small change in voltage corresponds to a very large change in current [26]. Like the non-thermal arcs, this arc also needs a more efficient electron emission to remain sustained, which is provided by field emission or thermal runaway [26]. Field emission and thermal runaway are referred to as cold emissions since they are independent of the cathode temperature [26, 12, 1]. However, field emission and thermal runaway can be assisted by temperature (heat load from the cathode), which gives us the thermo-field emission and we have the Schottky effect where the thermionic emission are assisted by the electric field.

3 Method

The method of conditional averaging is a simple statistical method used to find specific parts of a signal by imposing a condition on another correlated signal that recorded at the same time. It has earlier been employed by [14, 13, 20, 23] to find and study coherent structures within low-frequency electrostatic fluctuations and by [9] to find a two-dimensional coherent structure in turbulent plasma. In [23] this method were compared to a simple correlation analysis by using Monte Carlo simulation. They concluded the method of conditional analysis to be superior due to the fact the correlation analysis uses the square of the signal, making it insensitive to polarity. Additionally, the method of conditional analysis have been compared to numerical simulations in [14, 13, 20, 23, 9] and were concluded to be in good agreement. This method is briefly discussed in [14, 13, 20, 23, 9]. In this chapter, an elaborate introduction to this method is given with examples from [14, 13, 20, 23, 9].

3.1 Sampling process

The sampling process is performed by using two probes where one is a reference probe, denoted A and the other is a movable probe, denoted B. The reference probe is fixed in one position $\mathbf{r}_A$ measuring some quantity[1] $\phi_A(t, \mathbf{r}_A)$ while the movable probe can be moved to different selected positions $\mathbf{r}_B$ measuring the quantity $\phi_B(t, \mathbf{r}_B)$. The measured quantities ϕ_A and ϕ_B are regarded as random, correlated time series in statistical sense [14, 13, 20, 23, 9]. Random fluctuations within the plasma are assumed to be time-stationary[2] and homogeneous [14, 13, 20] in statistical sense such that the recorded time series on the spatial grid does not need to be taken simultaneously.

When a sufficient number of time series $\phi_A(t, \mathbf{r}_A)$ and $\phi_B(t, \mathbf{r}_B)$ are collected for the analysis, the movable probe moves to another selected position $\mathbf{r}_B = \mathbf{r}'_B$ and then the process repeats until a desired grid is obtained.

3.2 Condition

We define a condition C based on the characteristics of the structure we want to find and impose this condition on the time series from the reference probe ϕ_B [14, 13, 20, 23,

[1] The measured quantity, ϕ could be any plasma parameter, e.g fluctuations in potential, electron/ion temperature and density [14, 13, 20, 23, 9]

[2] A time-stationary process means the process carry the same mean and variance at all times i.e the joint probability distribution does not change when shifted in time [28]

9]. Whenever the time series from the reference probe satisfies the condition C, a time $t = t'$ is determined.

As an example, we look into two of the simplest conditions used by [14, 13, 20, 23, 9],

$$C_1 = \phi_C \qquad C_2 = n\sigma_A \tag{3.1}$$

where the first, C_1 is to look for some critical value ϕ_C, and the second C_2 is to look for some value larger than the average fluctuation level by using the standard deviation or the RMS value of the random fluctuations recorded by the reference probe, σ_A and multiply it with an integer n to make the condition C_2 larger than the random fluctuations. The usage of these conditions are straightforward; you find all occasions in the time series from the reference probe where the time series, ϕ_A are above some critical value ϕ_C or than the average fluctuation $n\sigma_A$. However, depending on the situation, using such simple condition given by equation (**??**) could make things more complicated than helpful. Consider $C_2 = n \cdot \sigma_A$, if n is a value too low, then C_2 may interpret noise as structure and if n is set too high, it may overshoot the actual structure we want to find [23]. A possible solution to this problem is to use a set of numbers $n \in [1, 2, ..., 5]$ then analyse each separately to find which is more successfull to find structure [23]. However, this will create more work thus consuming more time.

By employing several and more complicated conditions, then we can expect the resulting conditional average to be closer to the possible coherent structures [14]. This fact was demonstrated by numerical simulations [14, 13, 20]. As an example, we look into a set of more complicated conditions given by [14]

$$C_a = \phi_A < 0, \qquad C_b < \frac{d\phi_A}{dt}, \quad C_c = \nabla^2 \phi_A > 0 \tag{3.2}$$

where C_a is a condition which looks for occasions where the reference signal is negative, which can be defined to look for occasions where the reference signal is positive. C_b is the time condition, which looks for the occasion where the time derivative of the reference signal is negative. C_b can also look for occasion where the time derivative of the reference signal is positive. C_c is the spatial condition that looks for occasions where the double spatial derivative is positive. Some of the conditions shown by equation (**??**) were used by [13, 20, 23] in their study with space-time varying electrostatic fluctuations.

3.3 Conditional time Window

In **??** we discussed how the time, $t = t'$ is determined whenever the time series from the reference probe satisfies the applied condition, C. When this occurs, a conditional time window, C_τ of selected size is centred on that time [14, 13, 20, 23, 9]

$$C_\tau = [t' - \tau_1, t' + \tau_2] \tag{3.3}$$

where τ_1 and τ_2 are selected number depending on the interval the user desires, e.g. if the user wants an equally long interval on both sides of t', then $\tau_1 = \tau_2 = \tau$. The conditional time window is then imposed on the time series from the movable probe ϕ_A

to create the conditional time series[3]. The conditional time window can also be imposed on the time series from the reference probe to be analysed as well. These conditional time series can be written as

$$\begin{aligned} \phi_{A,C} &= (\phi_A|C) \\ \phi_{B,C} &= (\phi_B|C) \end{aligned} \tag{3.4}$$

3.3.1 Example: conditional time series

To give a better understanding to the subsequent sections, an example is presented. Figure **??** shows two real time series from [14] where A is from the reference probe and B is the time series from the movable probe. We observe in figure **??** the condition applied is $C = \phi_1$. When the reference probe satisfies this condition, a time $t = 0$ is determined, and a conditional time window of the selected and equal size, τ is centred on the time series from the movable probe, B

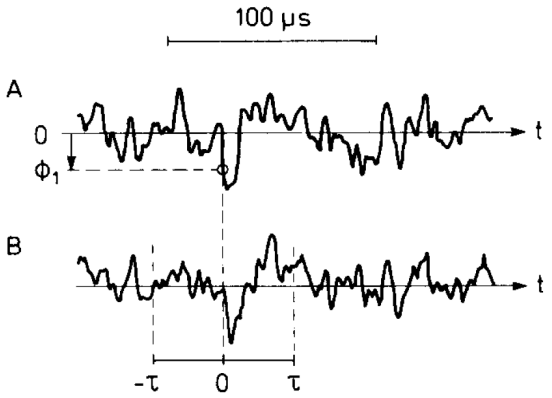

Figure 3.1: Illustration of the conditional sampling process with a single event (fig. 5 in [14])

3.3.2 Overlapping events

Whenever an event occurs that satisfies the applied condition, a conditional time window of selected size is centred at the time when the condition was satisfied. The next event that satisfies the condition needs to occur in a time such that its conditional time window does not overlap with the previous conditional time window, or the next one. Given we have non-overlapping conditional time windows, then the conditional time series $\phi_{A,C}$ and $\phi_{B,C}$ are considered independent realizations in statistical sense [13, 20]. This may be easier understood by the example given in section **??**

[3]Conditional time series are also referred to as sub-ensembles of the time series

3.4 Conditional analysis

When the conditional time series $\phi_{A,C}$ and $\phi_{B,C}$ are obtained, a statistical estimator can be applied to reduce noise (e.g. random fluctuations) and accentuate the structure. For this process, only two estimators were found to be usefull: The average and the median [14]. The average and median are both decent estimators for conditional analysis. However, the results obtained by using the average are easier to interpret physically than the median [14], hence the average is commonly employed for the analysis. The interested reader can find more details regarding the median as estimator in [14].

Furthermore, the average of a vector x is the sum of all vector elements in x, divided on the total number of elements in x [29]. This is usually denoted by a bar over the random variable or angle brackets, e.g. the $\bar{x} = \langle x \rangle$. The advantage of using the average other than being easily interpreted, is the fact that it minimizes the MSE[4] [14].

The conditional time series consists of N data sets per position of the movable probe. By averaging over all data sets, we obtain the conditionally averaged time series [14, 13, 20, 23, 9]

$$\begin{aligned} \bar{\phi}_{A,C} &= \langle \phi_A | C \rangle \\ \bar{\phi}_{B,C} &= \langle \phi_B | C \rangle \end{aligned} \tag{3.5}$$

3.4.1 Example: conditional averaging

To better understand the conditional averaging process, an example is presented. Figure **??** shows an example of the process of conditionally averaging a set of real time series from [23] from the reference- and movable probe. The top picture in figure **??** shows the time series from the reference probe. The dashed line is the applied condition, which in this case is $\phi < 2 \cdot \sigma$ where σ is the RMS value of the reference signal. We observe six cases where the time series from the reference probe satisfies the applied condition. In the second picture from the top in figure **??**, we have the conditional time windows at the movable probe. We observe the same six point in time where the reference signal satisfied the condition are selected as sub-ensembles from the total time series recorded by the movable probe. In the third picture from the top in figure **??**, we have the conditionally averaged time series from the reference signal. In the last picture in figure **??**, we have the conditionally averaged time series from the movable probe.

[4] MSE (mean square error) is the mean of all error from an estimator then squared [29]. We always want an estimator to carry a small MSE [29]

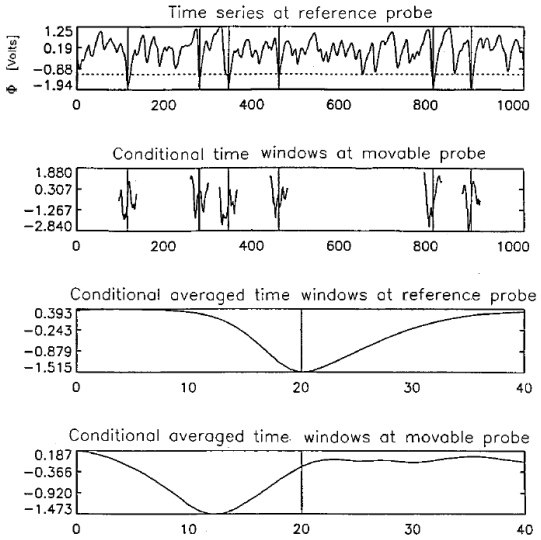

Figure 3.2: Illustration of conditional averaging with many events. The dashed line in the top plot illustrates the condition $C = 2 \cdot \sigma$ where σ is the RMS value of the reference probe (fig. 3 in [23])

4 Experimental set-up and recording

In this chapter, a description to the experimental set-up, how we achieved arcs with the set-up and how we recorded the time series for the analysis, is given.

4.1 Experimental set-up in SSC

The experiment was conducted in the Space Simulation Chamber (SSC), which is a cylinder shaped chamber with four ports, a main hatch at one end and a window at the other end for visual observation. Figure **??** (a) shows a schematic of the set-up as observed from the main hatch and (b) shows a schematic of the set-up as observed from the side. The gas supply used in this experiment is argon, and this gas is fed to the chamber through the main hatch, which is observed on the left side of figure **??** (b). The bottom port in figure **??** (a) and (b) we have the vacuum pump connected, which can create base pressure of $10^{-6}mbar$. The top port is also intended for another vacuum pump which were disconnected throughout the experiment.

The arcing set-up is located inside the chamber, between the ports in figure **??** (a) and (b). The electrodes used to create arcs consists of a anode needle and a cathode plate. The anode needle is connected to a high voltage cable, which is inside a grounded bore. The cathode plate is a grounded cathode aluminium plate with the area 10×10 cm, connected to a grounded rod. To keep the electrodes suspended in the middle of the chamber, between the ports, we installed a set-up consisting of two girders and a rail. On this rail, we connected the bore and the rod holding the anode and the cathode respectively. The rod and the bar are designed such that we can easily change the distance between the electrodes and their relative height inside the chamber, which is the Y-direction in figure **??** (a). The rail is designed such that we can easily move the electrodes in the axial direction, which is the Z-direction in figure **??** (a).

The high voltage set-up that delivers the high DC voltage to the anode is located outside the chamber, by the right port in figure **??** (a). The power supply used in the experiment is the model PS325 from Stanford Research Systems, which delivers $2.5kV$, $25W$ and $10mA$. However, like any other modern power supply, this one comes with a trip function[1], which is further discussed in section **??**. Moreover, the power supply is connected to a pulse generator by a coaxial cable and to the anode by a high voltage cable. Between the anode and the power supply, we have connected a $250k\Omega$ resistor and a high voltage probe. The probe is further discussed in section **??**. Furthermore, the power supply is connected a pulse generator, which is the model 81150A from Keysight.

[1] Trip is a function that shuts down the power delivered if the circuit becomes shorted. This is made to prevent the power supply to damage electrical components.

When the power supply receives a signal from the pulse generator, it will deliver the applied voltage to the anode.

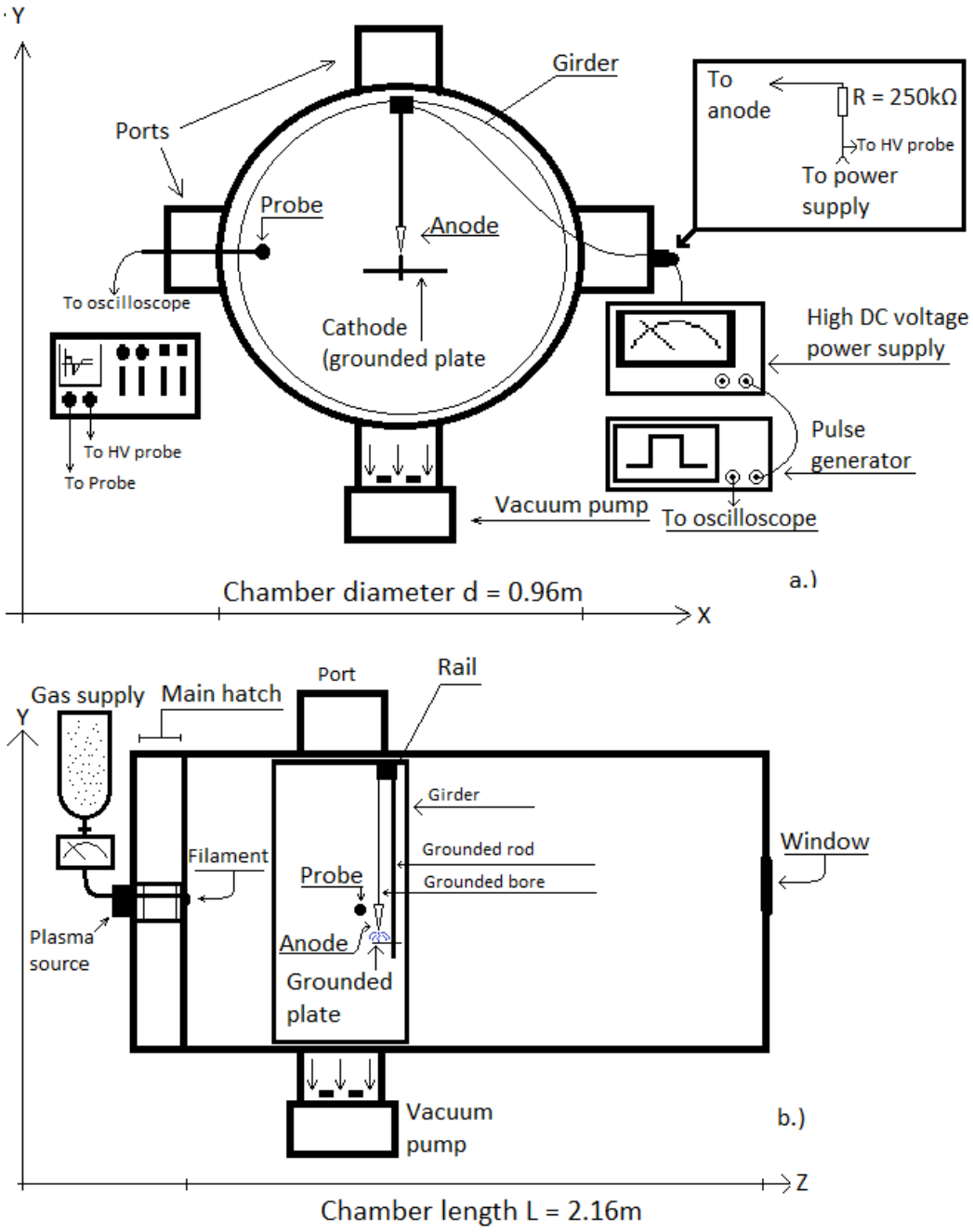

Figure 4.1: Experimental set-up in SSC observed from (a) the main hatch and (b) from the side.

The recording set-up consists of an oscilloscope, a reference probe and a movable probe. The oscilloscope is model MD3034 from Tektronix with $10^6\Omega$ and $13pF$ input termination and is located outside the chamber, by the left port in figure **??** (a). The reference probe is a high voltage probe, with the product name Agilent 10076B. This probe is located on the right port in figure **??** (a). The movable probe is a Langmuir probe with a spherical tip of the diameter $2mm$. The movable probe is located inside the chamber by the left port in figure **??** (a) and (b), denoted *probe*. The description of the actual recording of the time series is given in section **??**.

4.2 Arcing in SSC

In this section, a description to how we achieved optimal arcing for our analysis is given.

In the first series of testing, we attempted to achieve vacuum arcs, that is arcing without plasma. We set the distance between the electrodes to be $3.5cm$, the pulse length is set to $0.5s$, the base pressure is in the order of $10^{-6}mbar$, the pulse from the pulse generator was set to give a pulse of width $0.1s$ and the power supply was set to $2.5kV$ and $10mA$. The first problem we encountered was the power supply needs time to ramp up the voltage. The pulse had to be set to at least $0.5s$ such that the power supply manages to deliver the voltage. Furthermore, we achieved no arcing and no signal on the movable probe. We tested different electrode distances and tried to reduce the pressure by activating the gas flow stepwise from $0 - 20ccm$ where the pressure at $20ccm$ in the order of 10^{-5}. However, we still achieved no arcs. We think the applied voltage was not sufficient to create vacuum arcs, at least not at this pressure range.

For the second series of testing we set the electrode distance to be $1cm$ and we reduced the base pressure from 10^{-6} down to $2 \cdot 10^{-2}mbar$ by disconnecting the turbo pump and only using the pre-vacuum pump. However, at this pressure, the power supply began to trip, we reduced the current delivered down to $1mA$, restricting the power delivered to be $2.5W$. We increased the gas flow by one from $0ccm$ to $20ccm$ and we observed the discharges we achieved in the chamber. The most optimal in this case was the discharge we achieved with the gas flow at $5ccm$, which corresponds to the pressure $(4.2 \pm 0.2) \cdot 10^{-2}mbar$. When the pulse began, we observed a slight flash, followed by a glow-like discharge that surrounds the anode needle and stretches upwards along the bore. Before the pulse ended, we would occasionally achieve an arc on the bore, especially at the edges above the anode needle. We wanted to create the arcs between the anode needle and the cathode plate. We assumed the pressure was too low for the distance between the electrodes, and the edges on the bore grants a geometric field enhancement. We tried to isolate the edges on the bore and increase the distance between the electrodes. We tested for $5cm$ and $10cm$ distance between the electrodes, but still the same results, the arcs are now occurring on the bore where the isolation stops and we even have arcing on the bar holding the cathode plate. At this point, we decided to record the time series, in case we cant improve the set-up any further. Additionally, we found the recordings from the breakdown to have an arc-like behaviour, these are recorded as well. The records are presented and analysed in chapter **??**. While we had

a working set-up, we tried to change the polarity of the power supply and we did not observe any discharges at all.

For the third series of testing, we isolated the bore and the bar holding the cathode plate and we installed a needle on the cathode plate. We figure the cathode needle may give some geometric field enhancement to motivate an interaction between the anode needle and the cathode needle. However, at $1cm$, $5cm$ and $10cm$ electrode separation, we still had no interaction between them, we only achieved a glow discharge on the anode needle.

4.3 Arc recording

In this section, a description to how the time series were recorded with regards to the conditional sampling as explained in section **??**.

4.3.1 Conditional recording

To record the time series for conditional analysis, we used two probes, a reference probe and a movable probe. These probes were briefly introduced in section **??**, in this section we will explain their purpose.

The reference probe in this experiment is a high voltage probe that can monitor and record the high voltage delivered by the power supply. By monitoring the voltage delivered to the anode, we can use the location of the anode in the chamber as the reference position r_A.

The movable probe in this experiment is a Langmuir probe. The main purpose of this probe is to measure the ion and electron saturation current from a plasma cloud as it expands from the arcing. The saturation current collection is explained as follow. Given a plasma with the potential V_P. By applying a bias voltage, V_B much greater than the plasma potential, $V_B >> V_P$ then we will collect the electrons while repelling ions. This is process illustrated in figure **??**. The saturation current for the ion is collected by changing the polarity of the bias voltage applied on the probe. Assuming the velocity distribution of the electrons and ions are Maxwellian distributed, then the saturation current for the electrons and ions are given by [26, 18, 19] respectively

$$I_{es} = \frac{1}{4} e n_e v_{e,th} A_{probe} \tag{4.1}$$

$$I_{is} = \frac{1}{4} e n_i v_{i,th} A_{probe} \tag{4.2}$$

where e is the electron charge, n_e is the electron density, n_i is the ion density, A_{probe} is the surface area of the probe, $v_{e,th}$ and $v_{i,th}$ is the electron[2] and ion[3] thermal velocity

[2]The electron thermal velocity for a Maxwellian electron velocity is given by [26, 18, 19] $v_{e,th} \equiv \sqrt{8k_B T_e/\pi m_e}$ where K_B is the Boltzmann constant and m_e is the electron mass

[3]The ion thermal velocity for a Maxwellian electron velocity is given by [26, 18, 19] $v_{i,th} \equiv \sqrt{8k_B T_i/\pi m_i}$ where m_i is the ion mass

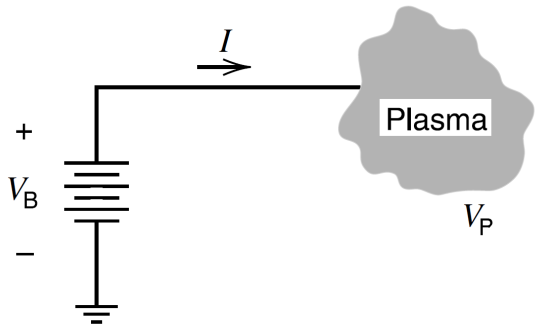

Figure 4.2: The definition of voltage and current for a Langmuir probe (fig. 6.5 from [18])

respectively. For more details regarding the Langmuir probe as a tool to diagnose the plasma is found in [26, 18, 19]. Furthermore, the bias voltage was set to $135V$ by coupling 15, $9V$ batteries in series. Additionally, we coupled a resistor, $R_e = 5.62k\Omega$ for electron current and $R_i = 10.9M\Omega$ for ion current, in series with the bias voltage to increase the resolution.

The data were recorded by the oscilloscope. We recorded $1M$ samples for all time series. The maximum sample frequency of the oscilloscope is $2.5GHz$, hence we recorded the electrons by this frequency. However, the ion sample frequency is from $100MHz$ to $500MHz$ since they have much larger structure, using a lower frequency would cause the measurements to be out of range. Furthermore, some measurements also have reduced number of batteries due to the peak of the current going out of range. Details on the frequency and number of batteries are given in chapter **??**.

4.3.2 Measurement grid

For the conditional analysis, we measured a 3×3 grid in the axial and radial positions, which is the X- and Z-direction in figure **??** (a) and (b). The recorded positions are summarized in table **??**. For each position, we recorded 20 time series for both currents and both arcs and breakdowns, which results in 80 time series per position. For future notice, the 10 *cm* axial has a 2.5 *cm* radial position instead of 0 *cm* since we feared this could initiate an arc between the movable probe and the anode.

Table 4.1: The axial and radial positions are noted in r while Δr is the distance between the electrodes to the radial probe, computed bu the Pythagorean theorem.

$r(axial, radial)$ $[cm]$	Δr $[cm]$
$(10, 2.5)$	10.31
$(10, 10)$	14.14
$(10, 20)$	22.36
$(20, 0)$	20.00
$(20, 10)$	22.36
$(20, 20)$	28.28
$(30, 0)$	30.00
$(30, 10)$	31.62
$(30, 20)$	36.05

5 Results and investigation

In this chapter, the time series recorded from the experiment are presented and investigated. Figure **??** shows two plots of the entire high voltage pulse where (a) shows the measured electron current and (b) shows the measured ion current. One should note that the order of magnitude in **??** (a) is different from **??** (b), and the reference curve on both plots are normalized accordingly.

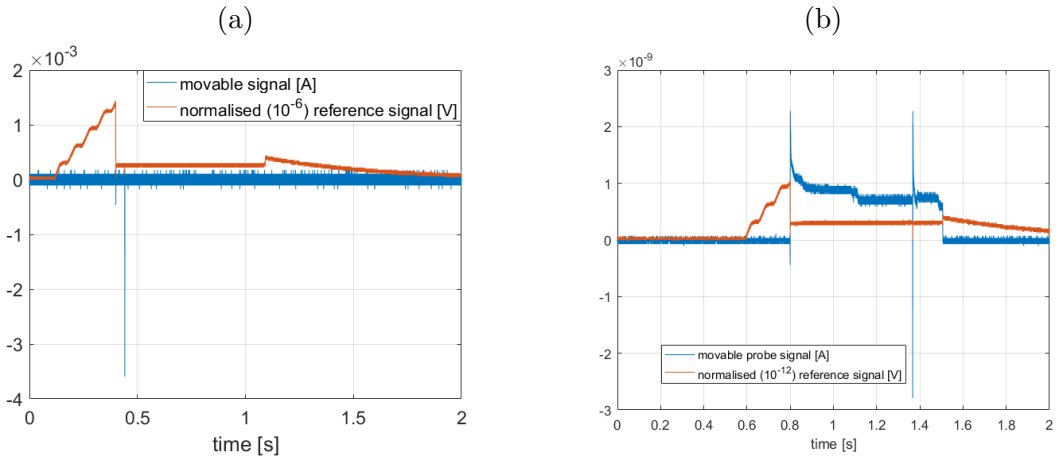

Figure 5.1: The whole high voltage pulse with (a) electron current and (b) ion current

In figure **??** we can observe the different regimes of the electrical discharges leading to an arc, as explained by section **??**. From the left in figure **??** we observe the voltage is slowly ramping up to the breakdown voltage of the gas, which occurs at random voltage values. When breakdown occurs, the voltage collapses down to $300V$ and we observe a glow discharge inside the chamber. At the same time as the breakdown occurs, we observe a negative current spike in figure **??** (a) and a negative, then positive current spike in **??** (b). These signals are not a part of our thesis, but since we discovered them, we will investigate parts of them. Furthermore, while the glow discharge is apparent in the chamber, an arc may occur at a random time. In figure **??** (a) the arc is observed as a large negative spike that occurs very soon after the breakdown, while in **??** (b) the arc is observed as a negative then positive spike current that occurs quite late in the pulse. When the high voltage pulse ends, the glow discharge dissipates.

In this chapter, we will investigate the arcs by means method of conditional averaging. The aim is to find the average structure of the electron and ion cloud and estimate their

expansion velocity. Additionally, we will look into the the time series obtained by the breakdown.

5.1 Arc analysis

In this section, we will investigate the arcs, observed as the second spike in figure **??** in (a) and (b). To avoid confusion, the electron and ion current are analysed separately in section **??** and **??** respectively.

5.1.1 Electron arc analysis

Figure **??** (a) and (b) shows three time series from the reference probe and the movable probe respectively. These time series were recorded in the axial position 10 cm and the radial position 20 cm with the frequency 2.5 GHz. The curve with the same color in figure **??** (a) and (b) corresponds to the same time series, e.g. the first time series is the blue curve in figure **??** (a) and (b). Furthermore, before the arc, the reference signal is constant at $300V$. During an arc, we observe in figure **??** (a) the reference signal drops sharply to the minimum of the curve, then climbs up slowly and linearly back to $300V$, while in in figure **??** (b) we observe the movable signal to drop sharply to a minimum of the curve, then relaxes towards zero current.

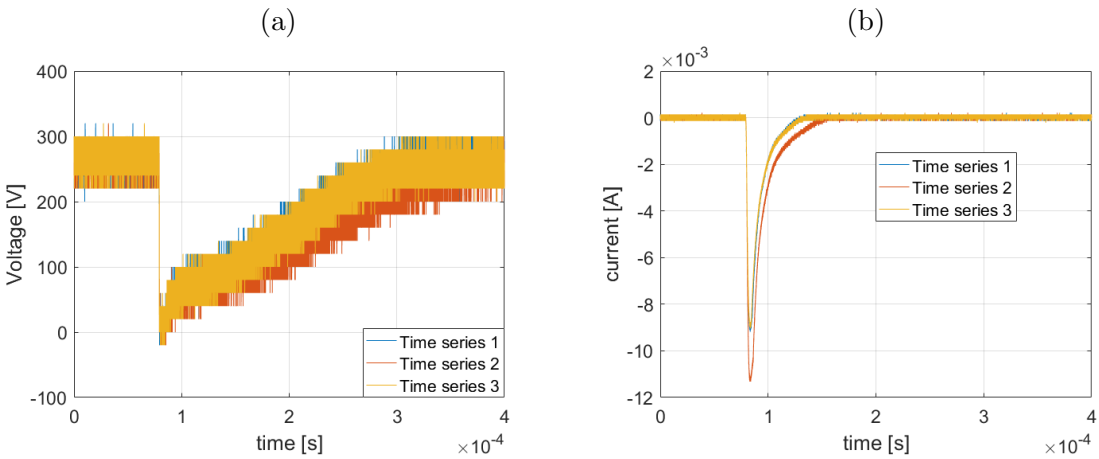

Figure 5.2: The arc observed by (a) reference probe [V] and (b) the movable probe [A] with 12 batteries voltage bias. These time series are recorded in the axial position 10cm and radial position 20cm with the sampling rate 2.5GHz.

We also have some recorded time series with double arcing, figure **??** shows an example this. The double arcing is characterized by carrying two minima where the second one appears some time later and are smaller. However, for the conditional analysis, we want

to find the typical shape of the electron cloud from a single arc, hence we remove the time series which has recorded double arcs.

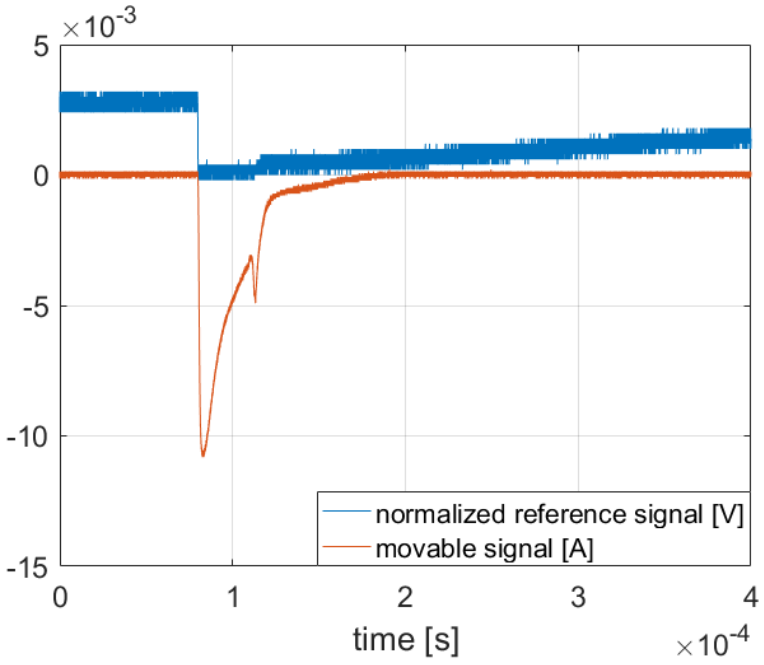

Figure 5.3: An example of an occurrence of double arcing. This time series is recorded in the axial position $10cm$ and the radial position $10cm$ with the sampling rate $2.5GHz$. The reference signal is normalized (10^{-6}) to be in scale with movable signal

The next step in this investigation is to apply the method of conditional averaging on the time series we have left to accentuate the typical shape of the electron current from a single arc plasma cloud. To use the conditional averaging, we need to impose a condition on the time series from the reference probe that determines the time when we have an arc. In figure **??** (a) we observe the reference signal has a rapid decay over a short time period. We determined this rapid decay to be the time when an arc occurs. To find the time of this rapid decay, we created a condition that locates the minima of the time derivative. Figure **??** shows the conditionally averaged time series for the electron currents from the whole grid with the number of batteries and number of time series used given. For the interested reader, the codes I developed to compute the conditional averaging is in the appendix **??**

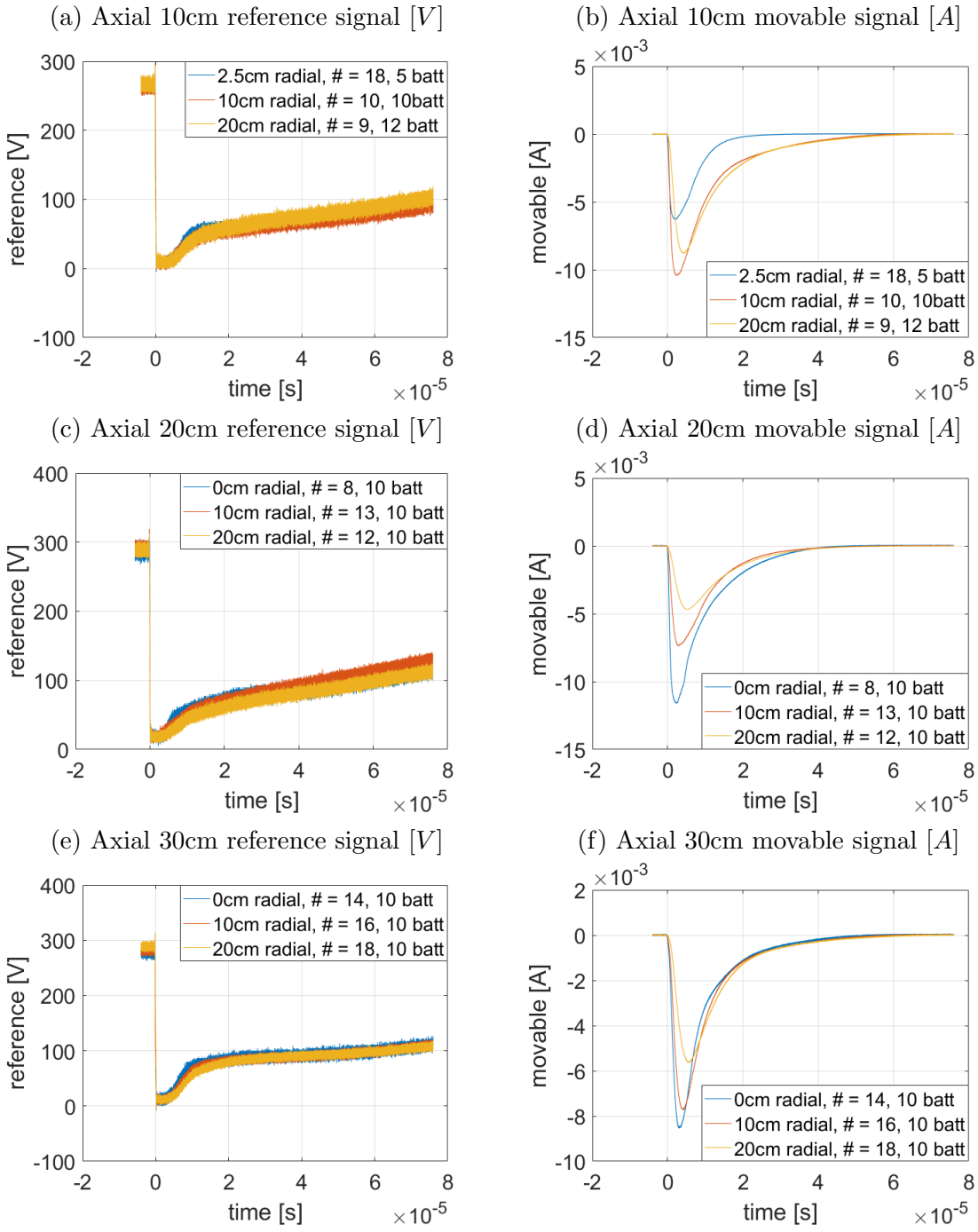

Figure 5.4: Conditionally averaged signals without double arcing. The reference signal [V] are shown in (a), (c) and (e) while the electron currents to the movable probe [A] are shown in (b), (d), (f). The conditional time window is 20% of the total time series. The number of time series used are indicated by #

By means of conditional averaging, the average shape of the electron cloud is given by figure **??** (b), (d) and (f), here we observe the curves to have a steep drop from zero current to a minimum, then relaxes towards zero current. We also observe the magnitude of the amplitudes from the electron clouds to be decreasing when the distance between the arcs and the movable probe increase in figure **??** (d) and (f), except for the signal at figure **??** (b), which appear to be anomalous.

The time delay is found by computing the time when the arc discharge is observed by the reference probe and the movable probe, then take the difference between them. However, the conditional analysis have already determined the time for when the arc discharge is observed by the reference probe, and that is at $t = 0$. We need to determine the time when the arc discharge passes the movable probe. We take the minimum of the time derivative of the conditional signal from the movable probe as an estimate for the time of arrival. This process is illustrated in figure **??** where the blue line is the conditionally averaged movable signal from the axial $10cm$ and radial $2.5cm$ position, while the red line is the time derivative of the same signal. The time derivative of the movable signal is normalized to be in scale.

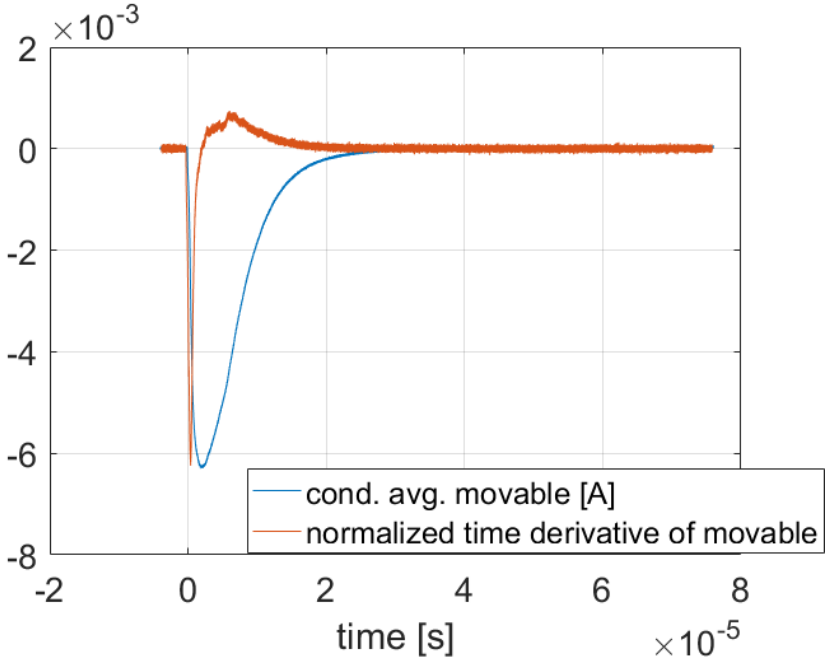

Figure 5.5: An illustration of the method to obtain the delay time to a given conditionally averaged signal. The blue line is the conditionally averaged movable signal while the red line is the normalized ($2{\cdot}10^3$) time derivative of the blue line. The minima of the red line determines the delay time of the blue line.

The average electron arc velocity, $\bar{v}_e$ can be estimated by computing the distance between the reference probe and the movable probe, then divide with the delay time between them. Table **??** summarises the position, distance between the probes, the

delay time and the velocity for the electron current from the arc. Figure **??** shows the correlation between the probe distance and the delay time. The slope of the line in figure **??** estimates the average velocity of the electron cloud expansion, which is $\bar{v}_e = 1.32 \cdot 10^6 ms^{-1}$

Table 5.1: Electron cloud properties

$r(axial, radial)$ $[cm]$	Δr $[cm]$	Δt $[s]$	$v = \Delta r / \Delta t$ $[ms^{-1}]$
$(10, 2.5)$	10.31	$0.0366 \cdot 10^-5$	281694
$(10, 10)$	14.14	$0.0506 \cdot 10^-5$	279447
$(10, 20)$	22.36	$0.1202 \cdot 10^-5$	186023
$(20, 0)$	20.00	$0.0406 \cdot 10^-5$	492611
$(20, 10)$	22.36	$0.0707 \cdot 10^-5$	316266
$(20, 20)$	28.28	$0.1544 \cdot 10^-5$	183161
$(30, 0)$	30.00	$0.1082 \cdot 10^-5$	277264
$(30, 10)$	31.62	$0.1471 \cdot 10^-5$	214956
$(30, 20)$	36.05	$0.1964 \cdot 10^-5$	183554

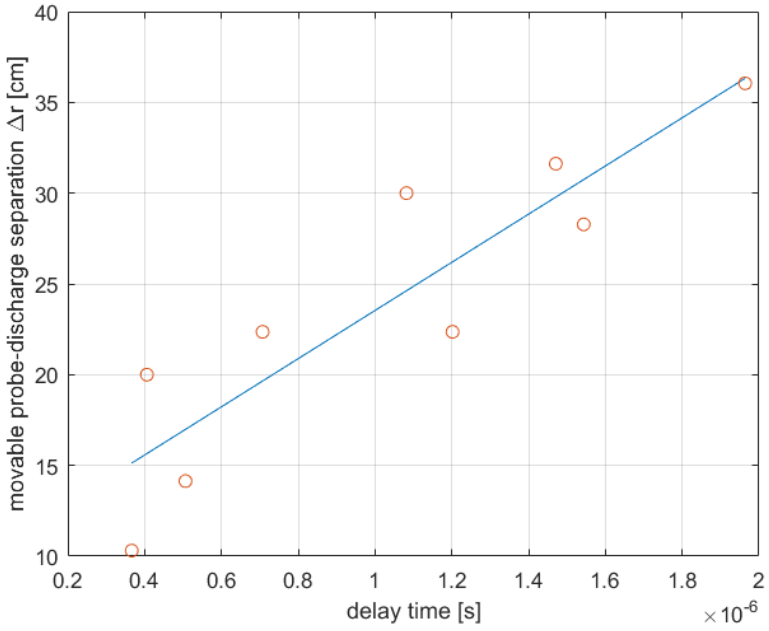

Figure 5.6: Scatter plot of the distance between the electrodes and the movable probe vs. time delay from the electron cloud.

5.1.2 Ion arc analysis

Figure **??** (a) and (b) shows three time series of the measured voltage and measured current respectively. These were recorded in the axial position $10cm$ and the radial position $20cm$ with the frequency 250 MHz. The same colors in figure **??** (a) and (b) corresponds to the same time series, e.g. the first time series is the blue curve in figure **??** (a) and (b). The time series 1 is shifted, which occurred due to a change in the trigger location of the oscilloscope during the experiment. Furthermore, we observe the voltage is constant at $300V$, as in the electron measurement. The measured current have some variation in amplitude as in the electron measurement, which we assume are due to arc occurring at different locations. We should note in **??** (b) before the arc, we are measuring a constant ion current from the glow discharge and when an arc occurs, we observe a negative spike, which we determined to be due to energetic electrons. When the negative spike hits a minimum, the curve raises exponentially above the steady ion current. This current above the ion current is interpreted as the ion cloud.

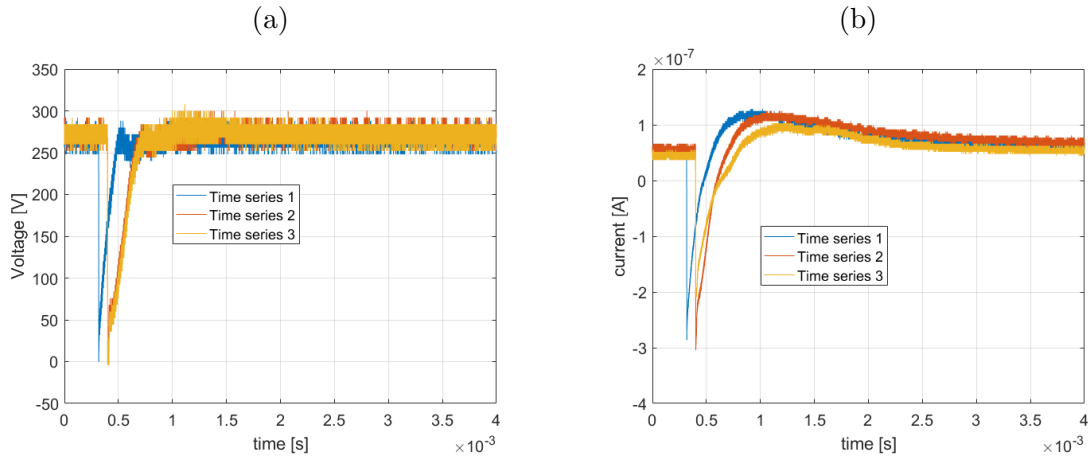

Figure 5.7: The arc observed in the axial position $10cm$ and radial position $20cm$ with the sampling rage $250MHz$ by (a) reference probe [V] and (b) the movable probe [A] with 15 batteries voltage bias.

The ion measurements are also affected by the double arcing, this is illustrated in fgure **??**. The characterization of the double arcing is a second, smaller minima after the first one, as in the electron measurement. For the conditional analysis, we removed the time series with double arcing since we want to obtain the shape of a typical ion cloud from a single arc.

Now we apply the method of conditional average on the time series we have left to accentuate the shape of the ion current from a single arc. The reference signal have the same characteristics as in the electron measurements, hence we can use the same condition. Figure **??** shows the conditionally averaged time series for the ion currents from the whole grid with the number of time series used given.

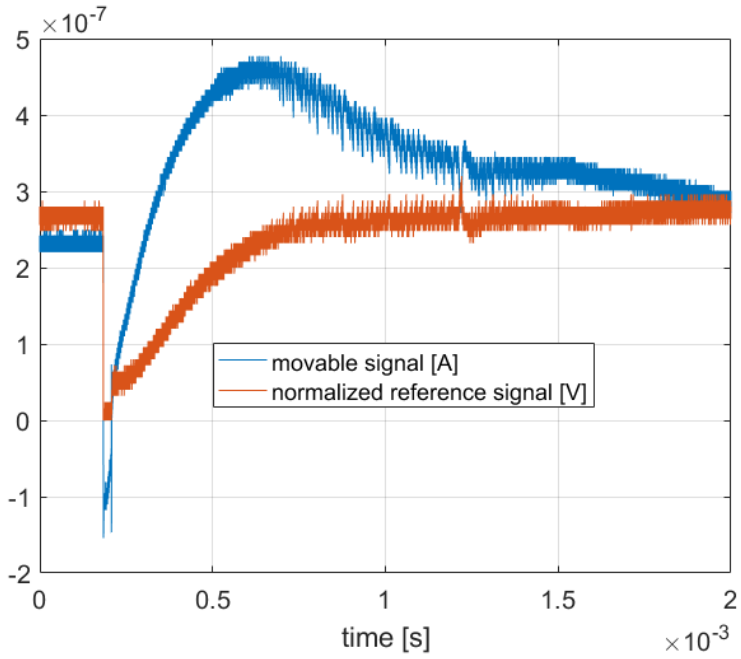

Figure 5.8: Example of double arc. This time series was recorded in the axial position $10cm$ and the radial position $2.5cm$ with the sampling rate 250 MHz. The blue line is the normalized (10^{-9}) reference signal $[V]$ and the red is the movable signal $[A]$ with 15 batteries

The average shape of the ion cloud can now be observed in figure **??** by the blue line, above the steady glow current. The shape of the ion cloud appears to be increasing logarithmic to a maximum, then relaxes toward steady state. We also observe a negative spike, which we interpret 0 as energetic electrons arriving before the ion cloud.

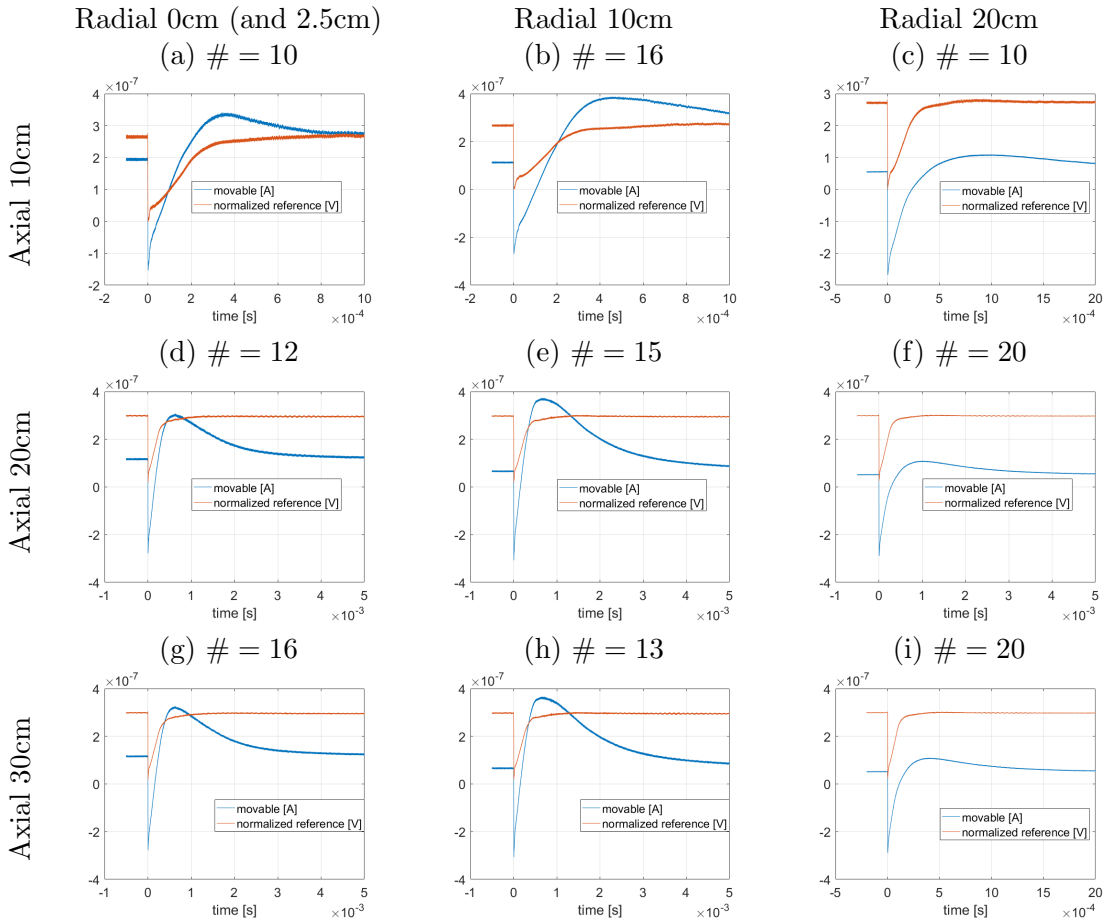

Figure 5.9: Conditional averaged time series without double arcing. The red line is the reference signal $[V]$ and the red line is the movable signal $[A]$, recorded with 15 batteries. The conditional time window is 50% of the total time series and the number of time series used are indicated by #

The time delay here cannot be estimated by the same method as in the electron arc analysis. We use the maxima of the conditionally averaged time series from the movable probe as the estimate for the arrival time. Table **??** summarises the position, distance between the probes, delay time and the velocity for all positions. Figure **??** shows the correlation between the probe distance and the delay time, which appears to have a large variation. The slope of the line estimates the average velocity of the ion cloud expansion, which is $\bar{v}_i = 119.2\ ms^{-1}$. This is a very low value compared to the values given by single positions in Table **??**, which is due to the large spread in figure **??**.

Table 5.2: arc ion

$r(axial, radial)$ $[cm]$	Δr $[cm]$	Δt $[s]$	$v = \Delta r/\Delta t$ $[ms^{-1}]$
$(10, 2.5)$	10.31	$0.3463 \cdot 10^{-}3$	297.7
$(10, 10)$	14.14	$0.4566 \cdot 10^{-}3$	309.7
$(10, 20)$	22.36	$0.8853 \cdot 10^{-}3$	252.6
$(20, 0)$	20.00	$0.6 \cdot 10^{-}3$	333.3
$(20, 10)$	22.36	$0.7 \cdot 10^{-}3$	319.4
$(20, 20)$	28.28	$1 \cdot 10^{-}3$	282.8
$(30, 0)$	30.00	$0.6283 \cdot 10^{-}3$	477.5
$(30, 10)$	31.62	$0.7062 \cdot 10^{-}3$	447.7
$(30, 20)$	36.05	$0.4054 \cdot 10^{-}3$	889.2

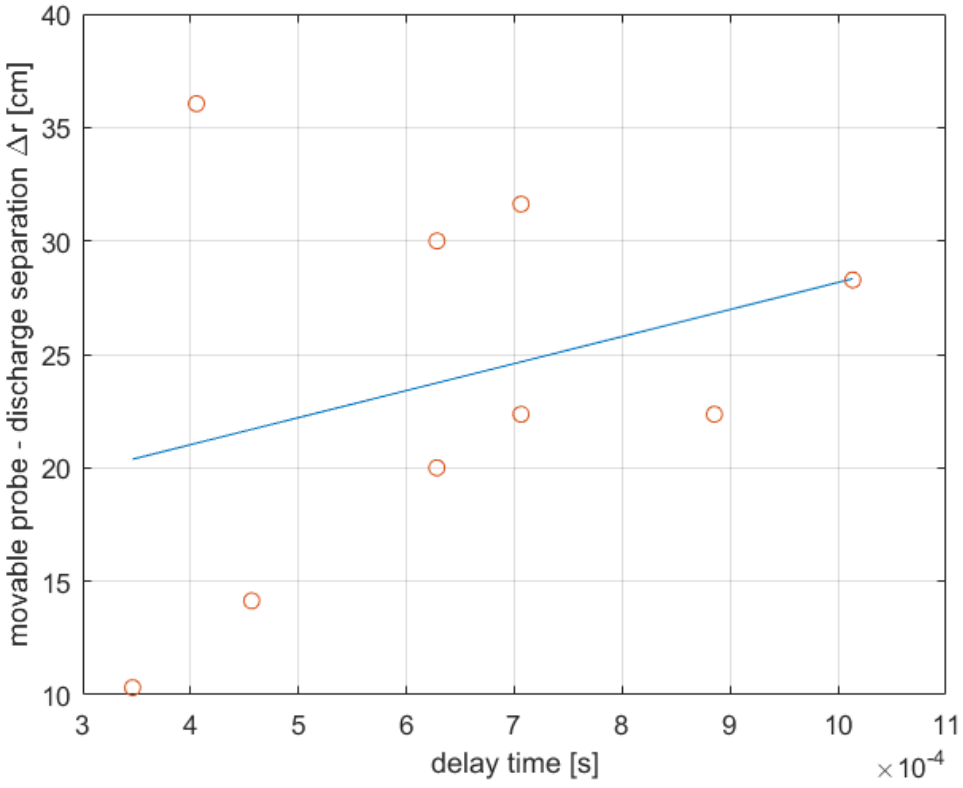

Figure 5.10: Scatter plot of the distance between the electrodes and the movable probe vs. time delay from the ion cloud.

5.2 Breakdown analysis

In this section, we will investigate the recorded time series of the breakdown, which is observed as the first spike in figure **??**. However, this investigation is beyond the scope of this thesis, hence the investigation here wont be extensive.

5.2.1 Electron Breakdown

Figure **??** shows three time series of the (a) measured voltage and (b) measured current. These time series were recorded in the axial position $10cm$ and radial position $20cm$, and sampled with the frequency $2.5GHz$. In figure **??** (a) we observe a high variation in the breakdown voltage, this is expected from the theory regarding electrical breakdown. Furthermore, we observe the magnitude of the voltage drop in figure **??** (a) is corresponding to the current amplitude in figure figure **??** (b). However, we do not observe any case of double arcing or anything alike, we assume all time series can be used for the conditional averaging.

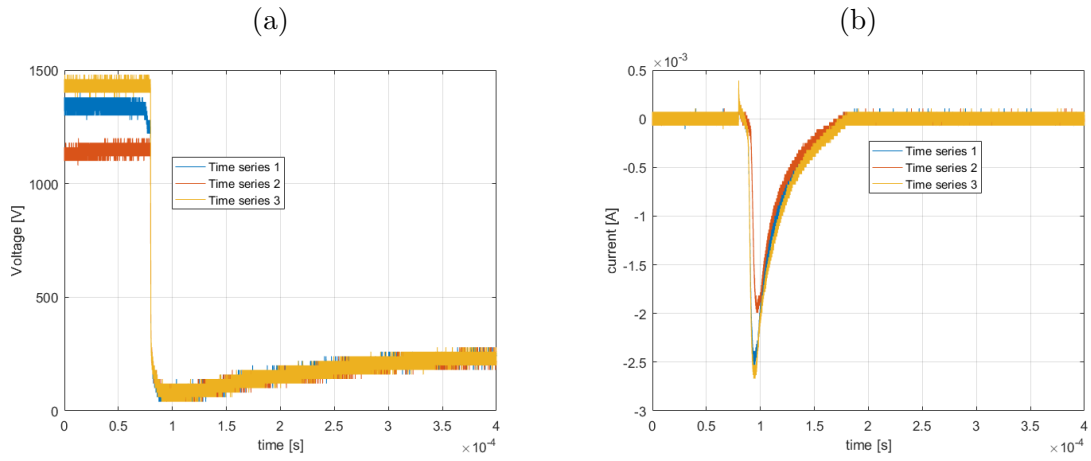

Figure 5.11: The breakdown observed in the axial position $10cm$ and radial position $20cm$ with high time resolution ($2.5GHz$ sampling rate) by (a) reference probe [V] and (b) the movable probe [A] with 15 batteries voltage bias.

For the conditional averaging, we observe the voltage to have the same rapid decay as the arc has, hence we can use the same condition we used in section **??**. The conditional averaged time series are given in figure **??**.

(a) Axial 10cm reference signal $[V]$

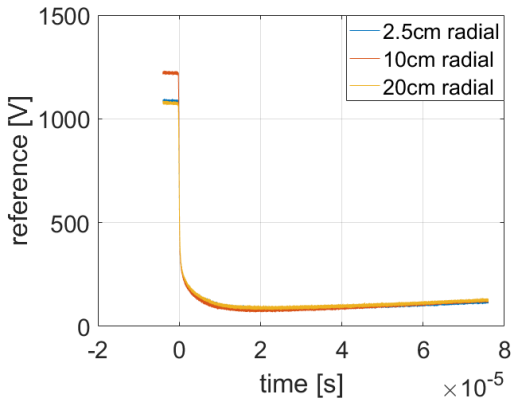

(b) Axial 10cm movable signal $[A]$

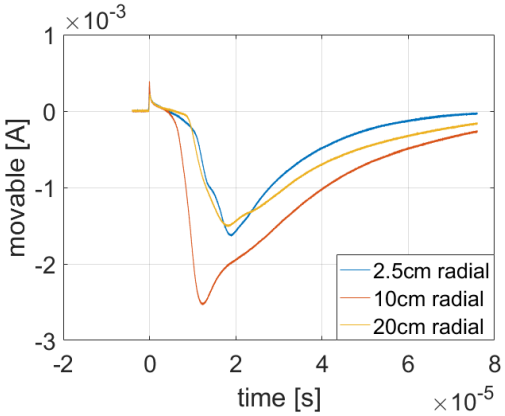

(c) Axial 20cm reference signal $[V]$

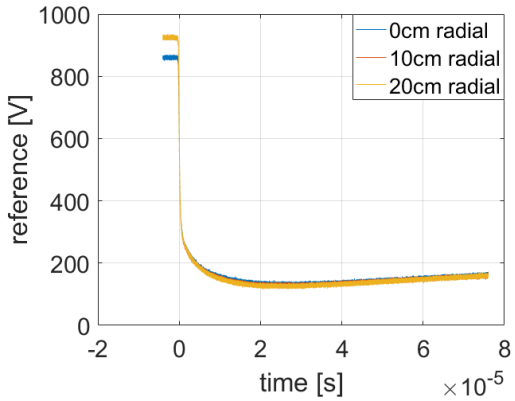

(d) Axial 20cm movable signal $[A]$

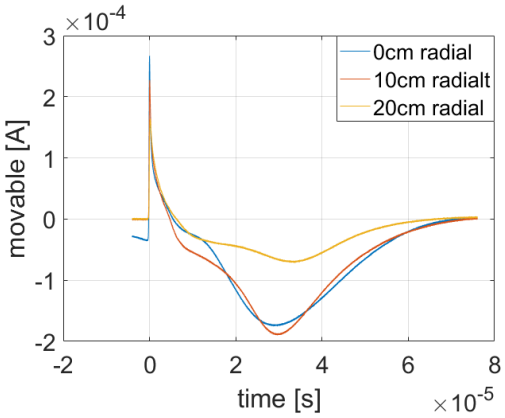

(e) Axial 30cm reference signal $[V]$

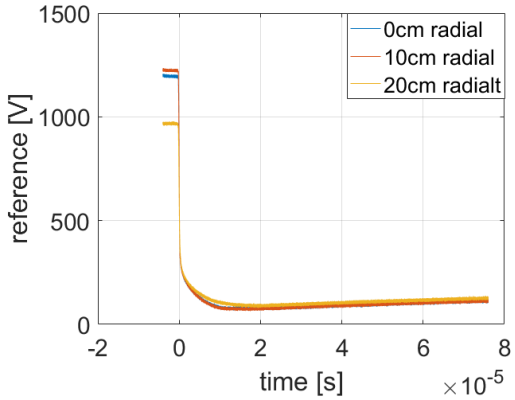

(f) Axial 30cm movable signal $[A]$

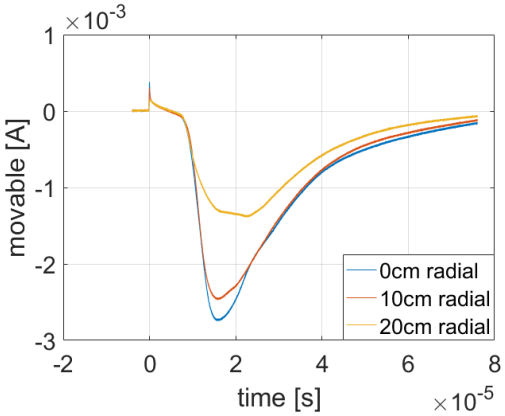

Figure 5.12: Conditionally averaged signals. The reference signal $[V]$ are shown in (a), (c) and (e) while the movable signals $[A]$ are shown in (b), (d), (f). The conditional time window is 20% of the total time from the time series. All time series have been used and all used 15 batteries.

Figure **??** (b), (d) and (f) shows the conditionally averaged movable signals, they have a very odd shape, as if they are distorted from their actual shape. It is readily observed that no singular shape is found and no systematic arrival time can be deduced, hence we need to find and impose another condition on the raw time series. Furthermore, the conditional averaged time series from axial 20 *cm* has a very low amplitude and a very different time of arrival compared to the others, hence we omit these from the investigation.

There appears to be a correlation between the breakdown voltage and the corresponding current amplitude in figure **??**. To show this, a few examples of scatter plot of the breakdown versus the minima of the current amplitude with a least square line is given in figure **??**

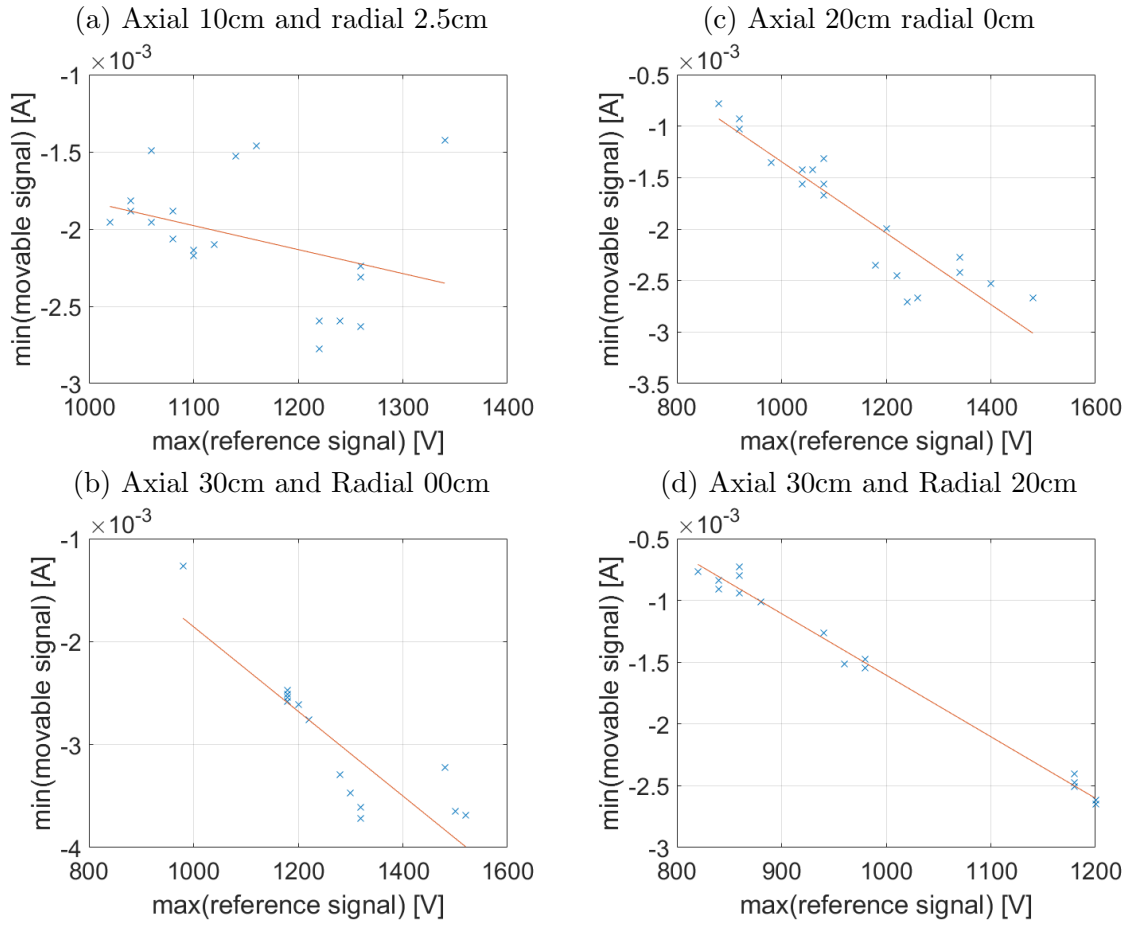

Figure 5.13: Scatter plots of breakdown voltage (the maxima of the reference signal) versus current amplitude (the minima of movable signal). A least square fit line is drawn to each scatter plot to illustrate the correlation.

In figure **??** we can also observe some clustering at certain breakdown voltages and

current regions, this is illustrated in figure **??**.

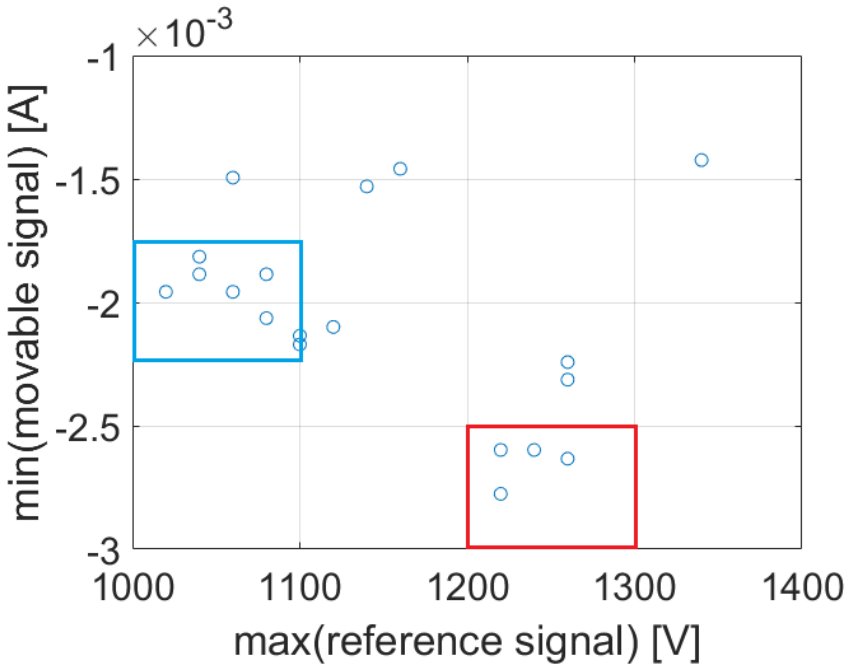

Figure 5.14: A scatter plot of breakdown voltage (the maxima of the reference signal) versus the current amplitude (the minima of the movable signal) from the position axial $10cm$ and radial $2.5cm$

We observe in figure **??** that we have clustering at two different voltage and current regions. These data sets are selected and we compute the conditional average of those, this is given in figure **??**

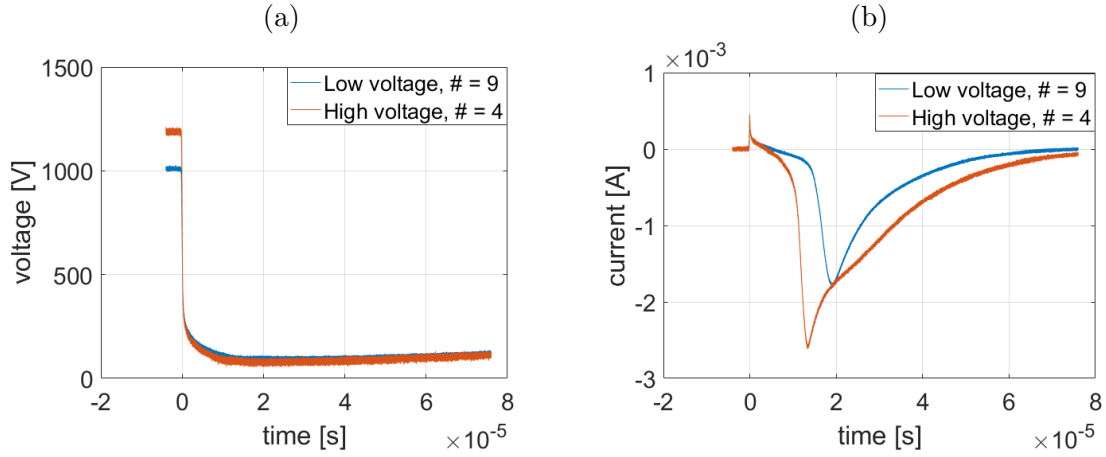

Figure 5.15: Conditionally averaged selected time series from axial $10cm$ and radial $2.5cm$ where (a) is the reference signal $[V]$ while (b) is current $[A]$. The # corresponds to the number of time series used.

Figure **??** reveals the time series with high breakdown voltage corresponds to high current amplitude and they give rise to an electron cloud which arrives faster. Assuming the breakdown occurs by the anode, then the distance between the breakdown and the movable probe is 10.31 cm. The delay time can be found by locating the minima of the time derivative of the conditional averaged time series, which is $t_L = 1.89 \cdot 10^{-5}\ s$ for the low voltage region and $t_H = 1.34 \cdot 10^{-5}\ s$ for the high voltage region. By dividing the distance on the delay time, we receive the velocities respectively, $v_L = 5441 ms^{-1}$ and $v_H = 7694 ms^{-1}$. As mentioned earlier, this investigation is beyond the scope of this thesis, therefore we will not investigate further.

6 Concluding remarks

The purpose of this thesis was to detect and diagnose plasma cloud formations from arcing between a needle anode and a cathode by means of conditional averaging.

We have found that electron cloud from the arcs are characterized by a steep drop from zero current to a minimum, then a relaxation back to zero current. Additionally, we found the magnitude of the amplitude to the electron cloud to be decreasing when the distance between the arc and the movable probe is increased. The average electron cloud velocity was found to be $\bar{v}_e = 1.32 \cdot 10^6\ ms^{-1}$

The ion cloud from the arcs were found to be characterized by a current above the steady state, which then increases logarithmically to a maximum, then relaxes back to steady state. However, the ion cloud measurement revealed a negative spike before the ion cloud, which indicates the electrons from an arc are energetic enough to be recorded by a negatively biased probe. The average ion cloud velocity was found to be $\bar{v}_i = 119.2\ ms^{-1}$, however the uncertainty was large due to high scattering.

We have discovered the breakdown of gas causes an arc-like behaviour of the electrons. By applying the method of conditional average, a distortion was revealed. This result led us to a new condition that revealed that a high voltage breakdown gives rise to an electron cloud the velocity $v_H = 7694ms^{-1}$, while the low voltage breakdown give rise an electron cloud with the velocity $v_L = 5441ms^{-1}$. Additionally, the amplitude on the electron cloud from the high voltage breakdown were significantly higher than the lower breakdown voltage. It is apparent the higher breakdown voltage creates a more energetic electron cloud than a lower breakdown voltage.

For future work regarding the breakdown, it is of interest to carry on the investigation I made through section **??**.

A Appendix

A.1 Matlab Codes for Conditional Averaging

This chapter introduces the two matlab codes I developed to compute the conditional averaged. Section **??** introduces the code developed to impose condition on the reference signal and then create the conditional time window, and **??** introduces the code developed to average the conditioned signals.

A.1.1 Conditional time interval

Figure **??** shows the matlab code for computing the conditional time window. The input vector x is treated by Savitzky-Golay filter by the matlab function $sgolayfilt$. This filter uses convolution as means to reduce the noise [22], which allows the original gradients of the curve to be preserved, e.g. if one uses normal moving average function then the gradients are heavily affected by the smoothing given by the moving average function. More information regarding this filter can be found in [22]. Furthermore, the filtered vector x is then taken the derivative of by the matlab function $diff$. This function computes the derivative by computing the difference $\Delta x_i = x_{i+1} - x_i$, which implies the output from this function generates a vector with one less element of the input, however, the loss of one element is considered insignificant since we recorded 10^6 samples (or vector elements). The min function is another matlab function that finds the global minima of the input. In this case, we use it to find the minima of the derivative of the input vector x, Δx_i. The outputs from this function are the vectors a and C, where a is the numeric value of the minima that we do not need, but necessary to make the function return the output C. C gives the vector element, $x_{i=C}$ which is the element containing the global minima, which is also the time $t = t'$ from the definition in section **??**. The next line is the conditional time window, here are the interval $C - \tau_1 < T < C + \tau_2$ created, as explained by **??**. In figure code: cond window I have selected $\tau_1 = 10^4$ and $\tau_2 = 1.9 \cdot 10^5$ which is used for the electron signals. The window is changed manually for the ions.

A.1.2 Conditional averaging

Figure **??** shows the matlab code for computing the average of the conditional time series. The inputs are the matrices x and y, where x is the reference matrix, while y is the signal matrix. Both matrices have the dimension mxn consisting of $m = 10^6$ data samples and $n = 20$ data sets. Furthermore, the first function $Cond_window$ finds the conditional time window vector to each data set n of the first or reference input x, and collects them into a matrix T. The next line imposes the conditional time window on the

```
function [T] = Cond_window( x )

    %Using Savitzky-Golay filter to remove noise - sgolay( vector,
 order, framelength )
    filt = sgolayfilt( x,1,1001 );

    %Defining the condition C
    [a,C] = min( diff( filt ) );

    %Defining the conditional time window
    T = [C-10000:C+190000];

end
```

Published with MATLAB® R2016b

Figure A.1: The conditional window matlab code

input matrix y. The output $cond_y$ is a matrix consisting the data samples $m(T) < m$ and the same number of data sets n. The last line compute the average of the input $cond_y$ by summing and dividing on the number of data sets n per data sample $m(T)$ within the conditional time window. This computation gives us the vector output $m(T)x1$.

```
function [ cond_avg ] = Cond_avg( x,y )

    %Collecting the conditional time windows
    for i = 1:size(x,2)
        [T(:,i)] = Cond_window( x(:,i) );
    end

    %imposing the conditional time window on the signal
    for i = 1:size(x,2)
        cond_y(:,i) = y(T(:,i),i);
    end

    %computing the conditional average of the signal
    cond_avg = ( sum( cond_y,2 ) )/size(cond_y,2);

end
```

Published with MATLAB® R2016b

Figure A.2: The conditional averaging matlab code

Bibliography

[1] André Anders. "Physics of arcing, and implications to sputter deposition". In: *Thin Solid Films* 502.1 (2006), pp. 22–28.

[2] Mark J Burchell, Mike J Cole, and PR Ratcliff. "Light flash and ionization from hypervelocity impacts on ice". In: *Icarus* 122.2 (1996), pp. 359–365.

[3] Mark J Burchell, L Kay, and P Ro Ratcliff. "Use of combined light flash and plasma measurements to study hypervelocity impact processes". In: *Advances in Space Research* 17.12 (1996), pp. 141–145.

[4] Mark J Burchell et al. "Hypervelocity impact studies using the 2 MV Van de Graaff accelerator and two-stage light gas gun of the University of Kent at Canterbury". In: *Measurement Science and Technology* 10.1 (1999), p. 41.

[5] DAVIDA CRAWFORD and PETERH SCHULTZ. "Laboratory investigations of impact-generated plasma". In: *Journal of Geophysical Research* 96.E3 (1991), pp. 18–807.

[6] DC Faircloth. "Technological aspects: high voltage". In: *arXiv preprint arXiv:1404.0952* (2014).

[7] GA Farrall. "Electrical breakdown in vacuum". In: *IEEE transactions on electrical insulation* 5 (1985), pp. 815–841.

[8] Alex Fletcher, Sigrid Close, and Donovan Mathias. "Simulating plasma production from hypervelocity impacts". In: *Physics of Plasmas* 22.9 (2015), p. 093504.

[9] Å Fredriksen et al. "Coherent structures, transport and intermittency in a magnetized plasma". In: *Plasma physics and controlled fusion* 45.5 (2003), p. 721.

[10] Joseph Fred Friichtenicht and John Charles Slattery. "Ionization associated with hypervelocity impact". In: (1963).

[11] Henry B Garrett and Albert C Whittlesey. *Guide to mitigating spacecraft charging effects*. John Wiley & Sons, 2012.

[12] Erhard Hantzsche. "Mysteries of the arc cathode spot: A retrospective glance". In: *IEEE transactions on plasma science* 31.5 (2003), pp. 799–808.

[13] T Huld et al. "Coherent structures in two-dimensional plasma turbulence". In: *Physics of Fluids B: Plasma Physics* 3.7 (1991), pp. 1609–1625.

[14] H Johnsen, HL Pécseli, and J Trulsen. "Conditional eddies in plasma turbulence". In: *The Physics of fluids* 30.7 (1987), pp. 2239–2254.

[15] Anton T Kearsley et al. "Laboratory simulation of impacts on aluminum foils of the Stardust spacecraft: Calibration of dust particle size from comet Wild-2". In: *Meteoritics & Planetary Science* 41.2 (2006), pp. 167–180.

[16] PJ Kellogg, K Goetz, and SJ Monson. "Dust impact signals on the wind spacecraft". In: *Journal of Geophysical Research: Space Physics* (2016).

[17] Attila Kohut et al. "Characterization of a copper spark discharge plasma in argon atmosphere used for nanoparticle generation". In: *Plasma Sources Science and Technology* 26.4 (2017), p. 045001.

[18] Michael A Lieberman and Alan J Lichtenberg. *Principles of plasma discharges and materials processing*. John Wiley & Sons, 2005.

[19] Robert L Merlino. "Understanding Langmuir probe current-voltage characteristics". In: *American Journal of Physics* 75.12 (2007), pp. 1078–1085.

[20] AH Nielsen, HL Pécseli, and J Juul Rasmussen. "Turbulent transport in low-β plasmas". In: *Physics of Plasmas* 3.5 (1996), pp. 1530–1544.

[21] P Oberc. "Electric antenna as a dust detector". In: *Advances in Space Research* 17.12 (1996), pp. 105–110.

[22] Sophocles J Orfanidis. *Introduction to signal processing*. Prentice-Hall, Inc., 1995.

[23] Frank J Øynes et al. "Experimental study of low-frequency electrostatic fluctuations in a magnetized toroidal plasma". In: *Physical Review E* 57.2 (1998), p. 2242.

[24] Paul R Ratcliff et al. "Experimental measurements of hypervelocity impact plasma yield and energetics". In: *International journal of impact engineering* 20.6-10 (1997), pp. 663–674.

[25] PR Ratcliff et al. "Velocity thresholds for impact plasma production". In: *Advances in Space Research* 20.8 (1997), pp. 1471–1476.

[26] J Reece Roth. *Industrial Plasma Engineering: Volume 1-Principles*. Vol. 1995. CRC press, 2001.

[27] DP Sheehan, CA Casey, and LT Volz. "Interaction of an expanding plasma cloud with a simple antenna: Application to anomalous voltage signals observed by Voyager 1, Voyager 2, ICE and Vega spacecraft". In: *Journal of Geophysical Research: Space Physics* 100.A10 (1995), pp. 19805–19808.

[28] Henry Stark and John William Woods. *Probability, statistics, and random processes for engineers*. Pearson, 2012.

[29] Ronald E Walpole et al. *Probability and statistics for engineers and scientists*. Vol. 5. Macmillan New York, 1993.